REVIEW

Perovskite Light-Emitting Diodes

small
methods

www.small-methods.com

Check for updates

Metal Halide Perovskites: From Crystal Formations to Light-Emitting-Diode Applications

Young-Hoon Kim, Sungjin Kim, Seung Hyeon Jo, and Tae-Woo Lee*

Metal halide perovskites (MHPs) are promising light emitters because they have high color purity, high charge-carrier mobility, comparable energy levels with organic semiconductors, and the possibility of diverse crystal forms and various crystal formation methods. Since the first report of MHP light-emitting diodes (PeLEDs) in 2014, many researchers have devoted efforts to increase the luminescence efficiencies of MHPs in various crystal forms, and achieved dramatically improved photoluminescence quantum efficiency of >90% in MHP emitters and external quantum efficiency of ≈14.36% in PeLEDs. Here, the recent progress regarding PeLEDs is reviewed by categorizing MHPs into three types: polycrystalline bulk films, colloidal nanocrystals, and single crystals. The main focus is on photophysical properties, crystallization methods, and mechanisms of various crystal formation, and applications to PeLEDs. Future research directions are also suggested and an outlook for MHP emitters and PeLEDs is given.

1. Introduction

Metal halide perovskites (MHPs) have superior optical and electrical properties, and are therefore being evaluated as light emitters for light-emitting diodes (LEDs)[1–4] and lasers.[5] MHPs have narrower emission linewidth (full width at half maximum (FWHM) ≤ 20 nm) and wider color gamut (≥140% of the National Television Standards Committee (NTSC) TV color standard)[1–4] than organic emitters (FWHM > 40 nm; color gamut cover < 100% of NTSC)[6–8] and inorganic quantum dots (QDs) (FWHM ≈ 30 nm; color gamut cover ≈ 100% of NTSC).[9–11] MHPs have also shown low lasing threshold (<600 nJ cm^{-2}) and extremely narrow lasing spectral linewidth (FWHM < 0.25 nm) above the lasing threshold.[12] Furthermore, these narrow emission linewidths in MHPs are not affected by the size of the grains or particles when they exceed the exciton Bohr diameter D_B.[1,13,14]

Dr. Y.-H. Kim, S. Kim, S. H. Jo, Prof. T.-W. Lee
Department of Materials Science and Engineering
Institute of Engineering Research
Research Institute of Advanced Materials
Nano Systems Institute (NSI)
BK21 PLUS SNU Materials Division
for Educating Creative Global Leaders
Seoul National University
1 Gwanak-ro, Gwanak-gu, Seoul 08826, Republic of Korea
E-mail: twlees@snu.ac.kr, taewkees@gmail.com

The ORCID identification number(s) for the author(s) of this article can be found under https://doi.org/10.1002/smtd.201800093.

MHPs conventionally are constituted by three atoms or molecules (here, we marked them as A, B, and X); A is an alkali metal cation (e.g., Cs$^+$) or organic ammonium (e.g., methylammonium (MA; CH$_3$NH$_3^+$), formamidinium (FA; CH(NH$_2$)$_2^+$), B is a transition metal cation (e.g., Pb^{2+}, Sn^{2+}, Mn^{2+}, Au^{2+}), and X is a halide anion (I$^-$, Br$^-$, Cl$^-$). These atoms or molecules can construct various MHP crystals with different dimensionalities such as ABX$_3$, A$_2$BX$_4$, A$_3$BX$_5$, and A$_4$BX$_6$: ABX$_3$ has a 3D structure in which the BX$_6$ octahedra are linked to each other three dimensionally;[2,3] A$_2$BX$_4$ has a 2D structure in which the PbX$_6$ octahedra are sandwiched between organic ammonium and form an infinite 2D plane;[15–17] A$_3$BX$_5$ has a 1D structure in which the PbX$_6$ octahedra share two opposite corners and form an infinite 1D chain;[18] A$_4$BX$_6$ has a 0D structure in which the PbX$_6$ octahedra are isolated in the organic ammonium or alkali metal cation matrix.[19,20] Especially, quasi-2D structures, which have various numbers of PbX$_6$ octahedral planes in MHPs, can be formed by incorporating 3D ABX$_3$ with 2D A$_2$BX$_4$; this structure has gained intensive attention for the emitting layer (EML) in high-efficiency perovskite LEDs (PeLEDs) these days as it has the 2D structure.[21,22] It is still under debate whether or not 0D A$_4$BX$_6$ crystals emit visible light.[19,20] MHP crystals with a 3D ABX$_3$ structure can also be formed having morphologically 1D chains and 2D nanoplatelets.[23] As dimensionality in MHP decreases from 3D (generally, ABX$_3$) to 0D (generally, A$_4$BX$_6$), the exciton binding energy E_B and bandgap gradually increase, whereas charge mobility tends to decrease.[24] Their color can be simply tuned over a wide range (380 ≤ λ ≤ 1000 nm) by substituting or partially mixing ion compositions. Furthermore, MHPs have great advantages such as low material cost, high charge-carrier mobility (e.g., electron mobility ≈ 1000 cm^2 V^{-1} s^{-1} in CsPbBr$_3$ single crystals),[25] comparable energy levels with organic semiconductors (e.g., conduction band minimum (CBM) ≈ 3.6 eV and valence band maximum (VBM) ≈ 5.9 eV in MAPbBr$_3$; CBM ≈ 3.6 eV and VBM ≈ 5.6 eV in MAPbI$_3$),[2,26] and low energy disorder.[27] Therefore, MHPs have been studied as alternative light emitters for natural-color displays.

Despite these advantages, high-efficiency LEDs based on polycrystalline (PC) MHPs are not easily achieved, because they have: i) low photoluminescence quantum efficiency (PLQE)[13] and ii) rough surface with many pinholes and defects, which severely increase the leakage current and

**ADVANCED
SCIENCE NEWS**

www.advancedsciencenews.com

**small
methods**

www.small-methods.com

reduce the electroluminescence (EL) efficiency in PeLEDs.[4,28] Thus, initial PeLEDs based on MHP PC films (early 1990s) showed bright EL only at low temperature of ≈77 K, or were too dim at room temperature (RT) to enable quantification of device efficiency,[15–17] and therefore did not attract the interest of researchers.

In 2014, Tan et al. fabricated thin MHP PC films and used them to achieve PeLEDs that are bright at RT: green light with external quantum efficiency (EQE) ≈ 0.1%, current efficiency (CE) ≈ 0.3 cd A^{-1}, and luminance L ≈ 364 cd m^{-2}; and near-infrared (NIR) lights with EQE ≈ 0.76% and radiance ≈ 13.2 W sr^{-1} m^{-2}.[3] Then, Kim et al. demonstrated bright PeLEDs based on MHP PC films with EQE ≈ 0.125%, CE ≈ 0.577 cd A^{-1}, and L ≈ 417 cd m^{-2} by facilitating hole injection into MHP PC films and preventing luminescence quenching at the interface between the hole injection layer (HIL) and the MHP PC films.[2] These devices still showed much lower EL efficiency than did inorganic QD LEDs[29,30] and organic LEDs (OLEDs);[8,31,32] however, they were enough to demonstrate the possibility of achieving high EL efficiency in MHP emitters, and to stimulate interest from researchers.

Low EL efficiency of MHP emitters has been overcome by developing and modifying various forms of MHP emitters such as: i) MHP PC films, ii) MHP nanocrystals (NCs), and iii) MHP single crystals (SCs) (**Figure 1**). Basically, the PLQE of MHP emitters can be increased by reducing the dimensionality of crystals[33] or the size of the perovskite grains[1,4] that confine the electron-hole pairs, and by reducing trap density.[34] The EL efficiency of PeLEDs can be increased by fabricating uniform perovskite layers in order to reduce the leakage current in devices.[4] Therefore, to efficiently confine charge carriers, suppress trap states, prevent a leakage current, and increase the EL efficiency of PeLEDs, researchers have used diverse crystal-formation methods (e.g., the solution process,[1–4] vacuum deposition,[35–39] the vapor-assisted solution process (VASP),[40–42] and crystallization assisted by microwaves,[43] by sonication,[44] or by mechanical milling[45]). These intensive and diverse efforts have achieved MHP emitters with dramatically increased EL efficiencies (EQE ≈ 14.36% in green-emitting PC films,[46] EQE ≈ 10.4% in green-emitting PC films,[47] EQE ≈ 8.73% in green-emitting NCs,[48] and EQE ≈ 0.1–0.2% in SCs).[49]

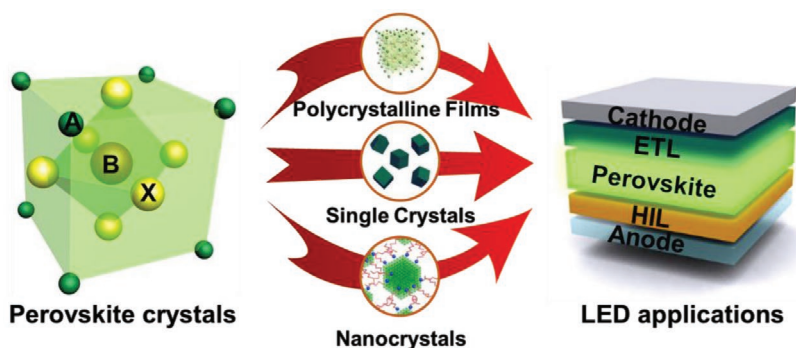**Young-Hoon Kim** received his M.S. (2014) in the Division of Environmental Science and Engineering and Ph.D. (2016) in material science and engineering from the Pohang University of Science and Technology (POSTECH), South Korea. He is currently working in materials science and engineering at the Seoul National University, South Korea as a postdoctoral researcher (2016–2018). His research focuses on solution-processed electronics based on organic and organic–inorganic hybrid materials for flexible displays and solid-state lightings.

Tae-Woo Lee is an associate professor in materials science and engineering at the Seoul National University, South Korea. He received his Ph.D. in chemical engineering from the KAIST, South Korea in 2002. He joined Bell Laboratories, USA as a postdoctoral researcher and worked at Samsung Advanced Institute of Technology as a member of research staff (2003–2008). He was an associate professor in materials science and engineering at the Pohang University of Science and Technology until August 2016. His research focuses on printed electronics based on organic and organic–inorganic hybrid materials for flexible displays, solid-state lighting, and solar-energy-conversion devices.

Here, we review this rapid development of MHP emitters, and demonstrate their great potential as light emitters. We categorize the crystal forms into: i) PC bulk films, ii) NCs, and iii) SCs (**Figure 2**). In Sections 2 and 3, we provide the recently reported solution and vacuum-deposition processes, respectively, that have been used to fabricate uniform MHP PC films and high-efficiency PeLEDs. In Section 4, we review the various methods to synthesize MHP NCs, and recent advances in PeLEDs based on them. In Section 5, we cover the synthesis of MHP SCs and their application in LEDs. Finally, we provide insights and future research directions to develop MHP emitters that can achieve highly efficient PeLEDs.
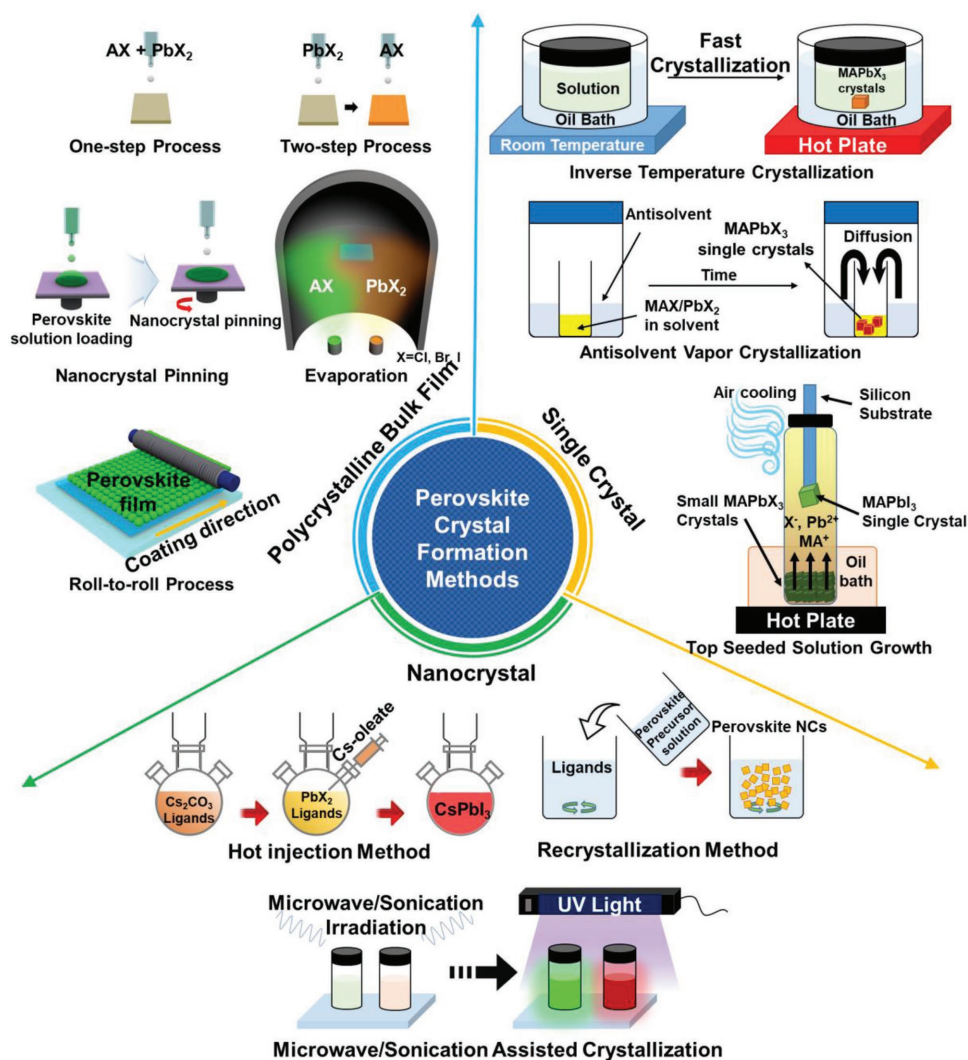

Figure 1. Schematic illustration describing the application of various perovskite crystals to light-emitting diodes.

Figure 2. Schematic illustrations of various perovskite crystal formation methods.
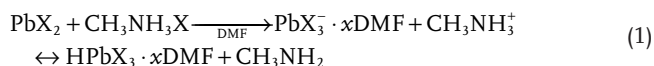
2. Solution-Processed Polycrystalline Bulk Films and Light-Emitting Diodes

MHP PC bulk films can be easily fabricated by coating and drying the perovskite precursor solutions, so solution-processed MHP PC films were first developed as an EML in PeLEDs. To increase the EL efficiency of MHP PC films, chemical, photophysical, and morphological properties such as surface morphology, thickness, and grain size of MHP PC films have been modified by controlling the precursor ratio,[50] by using additives that delay or prevent crystal growth,[51,52] by mixing various types of organic ammonium,[21,22] or by dripping volatile solvent on the spinning perovskite quasi-film.[4] Especially, researchers have mainly tried to increase the morphological uniformity, reduce the dimensionality, and decrease the grain size in PC films because: i) PLQE of MHP PC films can be increased by confining electron-hole pairs in low-dimensional crystals or in small perovskite grains,[4,33] and ii) EL efficiency of PeLEDs can be increased by fabricating uniform perovskite layers to reduce leakage current in devices.[4] In this section,
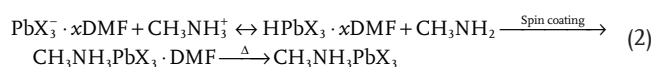
we review recently reported fabrication methods of solution-processed MHP PC films and PeLEDs based on them.
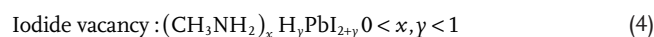
2.1. One-Step Solution Process

The one-step solution process is the simplest solution-process method to fabricate MHP PC films, so it was first used to fabricate PC films and PeLEDs. Perovskite solution is prepared by dissolving appropriate molar ratios of AX precursor and BX_2 precursor in polar solvents. Because MHP crystals have high dipole moments μ (e.g., $MAPbI_3$ has $\mu \approx 1.94$ D as measured by impedance spectroscopy, or $\mu \approx 2.1$ D as estimated using ab initio electronic structure calculation),[53–56] they can be dissolved only in polar solvents with high μ, such as N,N-dimethylformamide (DMF) ($\mu \approx 3.86$ D), dimethylsulfoxide (DMSO) ($\mu \approx 3.96$ D), and γ-butyrolactone (GBL) ($\mu \approx 4.27$ D). Perovskite precursors (here, CH_3NH_3X, PbX_2) were dissolved in polar solvents as colloidal dispersions with new coordination following this reaction pathway[40,57,58]

ADVANCED
SCIENCE NEWS
www.advancedsciencenews.com

small
methods
www.small-methods.com

$$PbX_2 + CH_3NH_3X \xrightarrow{DMF} PbX_3^- \cdot xDMF + CH_3NH_3^+$$
$$\leftrightarrow HPbX_3 \cdot xDMF + CH_3NH_2 \quad\quad (1)$$

PbX_2 was dissolved in solution by making soft coordination with CH_3NH_3X or DMF; as the amount of CH_3NH_3X increased, the solubility of the PbX_2 increased due to halide coordination of Pb^{2+}; this trend indicates that the size of colloids in solution and the final film morphology can be controlled by adjusting the ratio of CH_3NH_3X (MAX) to PbX_2.[58] During the first stage of the spin-coating process, the centrifugal force flings the dispensed solvent off the edge of the wet film. As the solvent begins to evaporate and perovskite solution concentration increases to exceed supersaturation, PbX_2 with lower solubility in polar solvent crystallizes first, then reacts with MAX, which has higher solubility in solvent; the result is $CH_3NH_3PbX_3 \cdot DMF$ coordination that can provide nucleation sites for crystal growth (**Figure 3**a).[40,57–59]

$$PbX_3^- \cdot xDMF + CH_3NH_3^+ \leftrightarrow HPbX_3 \cdot xDMF + CH_3NH_2 \xrightarrow{\text{Spin coating}}$$
$$CH_3NH_3PbX_3 \cdot DMF \xrightarrow{\Delta} CH_3NH_3PbX_3 \quad\quad (2)$$

As the coating process proceeds, perovskite crystals grow until all remaining solvent has evaporated. Annealing after this nucleation scheme yields MHP PC films.[40,57,58] Kim et al. and Tan et al. reported the first bright inverted PeLEDs and normal PeLEDs by using this one-step solution process.[2,3] However, MHP PC films fabricated by this process have a rough surface morphology with large cuboidal crystals of size greater than micrometers, due to: 1) fast and abrupt crystallization, 2) different solubility between PbX_2 and MAX,[60] and there are possible impurities in the formed crystals as below[57]

$$CH_3NH_2 \text{ vacancy} : (CH_3NH_2)_x HPI_3 \quad\quad (3)$$

$$\text{Iodide vacancy} : (CH_3NH_2)_x H_y PbI_{2+y} \, 0 < x, y < 1 \quad\quad (4)$$

All of these factors severely reduce the PLQE and EL efficiency of MHPs in PeLEDs. These indicate that the crystallization rate, the solubility difference between the perovskite precursors (e.g., PbX_2 vs MAX), and impurities in the formed crystals should be controlled to increase both the PLQE and EL efficiency of MHP PC films. Thus, many researchers have tried
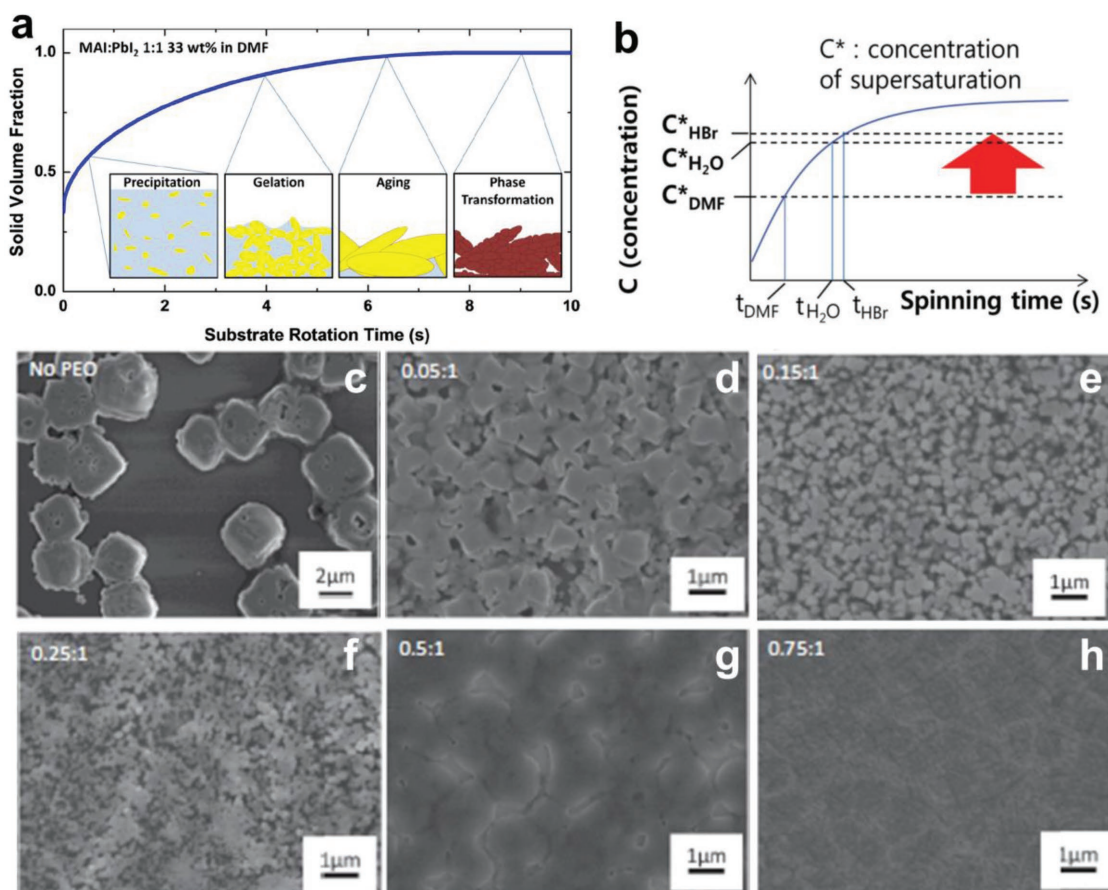

Figure 3. a) Schematic image illustrating the film formation process of one-step solution process. Reproduced with permission.[59] Copyright 2018, the Royal Society of Chemistry. b) Schematic illustration for the one-step solution process with crystallization-preventing additives. Reproduced with permission.[28] Copyright 2014, Wiley-VCH. c–h) SEM image of PEO:MAPbBr3 polycrystalline films with different PEO:MAPbBr3 ratios. Reproduced with permission.[52] Copyright 2015, Wiley-VCH.

**ADVANCED
SCIENCE NEWS**
www.advancedsciencenews.com

**small
methods**
www.small-methods.com

to improve the MHP PC film morphology by: i) controlling the precursor ratio, ii) increasing the film density, iii) preventing crystal growth, and iv) increasing the nucleus numbers.

2.1.1. Precursor Ratio Control

Poor morphology of MHP PC films occurs because PbX_2 has lower solubility than AX in solvent, and reduced number of coordination complexes of lead polyhalides induces huge colloidal soft frameworks in solution and large PbX_2 impurities in the final films.[57,58] Therefore, the film morphology can be improved by finely controlling the precursor ratio between AX and PbX_2. Increasing the ratio of AX to PbX_2 in the perovskite solution increases the coordination number of the lead polyhalides with AX and thus reduces the colloid size in solution and reduces the grain size in the resultant MHP PC films.[58] As the molar ratio of MABr increases from 1:1 to 2.2:1, the morphology of the $MAPbBr_3$ PC films improves and the perovskite grain size decreases.[61] However, if the molar ratio of MABr to $PbBr_2$ is too high (MABr:$PbBr_2$ = 3:1), the excess MABr retards the crystallization of the perovskite by inducing dewetting of the perovskite grains from the underlayer and thereby causes the formation of large aggregated $MAPbBr_3$ crystals. At the optimal MABr:$PbBr_2$ ratio (2.2:1), PL intensity, and PL lifetime greatly increased; this observation indicates suppression of nonradiative recombination and passivation of defects in $MAPbBr_3$ PC films. $MAPbBr_3$ PeLEDs with MABr:$PbBr_2$ = 2.2:1 had EQE ≈ 3.38%, CE ≈ 15.26 cd A^{-1}, and L ≈ 6124 cd m^{-2}; these were orders of magnitude higher than those of PeLEDs with MABr:$PbBr_2$ = 1:1 (EQE ≈ 0.004%, CE ≈ 0.02 cd A^{-1}, L ≈ 28.8 cd m^{-2}). Another report in the literature, which demonstrated high-efficiency PeLEDs based on in situ-formed NCs demonstrated that the optimal MABr:$PbBr_2$ ratio was 3:1;[62] this indicated that the optimal MABr:$PbBr_2$ ratio can be different according to the film formation process and crystal forms. Excess MABr also increased the luminescence efficiency (LE) of mixed halide PC films ($MAPbBr_xCl_{3-x}$).[50] The halide anion composition of the perovskite structure also affects the surface morphology because the nucleation rates differ among PbX_2 halides.[58,63,64]

Control of the perovskite precursor ratio can also be effective to improve the film morphology and LE of all-inorganic $CsPbBr_3$ PC films. As the molar ratio of CsBr increased in the precursor solution, the PL lifetime and the PLQE of $CsPbBr_3$ films increased from 5.06 to 45.7 ns and from 0.5% to 33.6%, respectively, due to the passivation of surface traps and reduced nonradiative recombination. As a result, EL efficiencies (CE ≈ 0.57 cd A^{-1}, L ≈ 7276 cd m^{-2}) with high operating stability under the ambient air (L > 100 cd m^{-2} for > 15 h) were achieved.[65]

2.1.2. Crystallization-Delaying Additives

The rough surface morphology of MHP PC films occurs mainly as a result of the fast and abrupt crystallization during spin coating.[28] Thus, MHP PC films can be smoothened by adding liquid additives that have low vapor pressure P_{vapor} to the perovskite solutions. A small amount of liquid additives with low P_{vapor}

(e.g., N-cyclohexyl-2-pyrrolidone (CHP) (P_{vapor} ≈ 0.05 mmHg at RT),[66] 1,8-diiodooctane (DIO) (P_{vapor} ≈ 0.000281 mmHg at RT)[67]) reduce the evaporation rate of polar solvent (e.g., DMF) and crystallization rate of perovskite crystals, and thus enable homogeneous nucleation and development of smooth MHP PC film that covers the substrate completely.[60] Especially, DIO additives induced intermediate states, such as chelation of Pb^{2+} with iodocarbons in DIO, and thus further delay the crystallization of perovskite crystals. Adding a solid additive, NH_4Cl, into the perovskite precursor solution can also retard the crystallization of the perovskite precursors by inducing intermediate states (e.g., $PbX_2 \cdot MAX\cdots x \cdot NH_4Cl$).[68] These additives can be removed during spin coating, or by postannealing.

Addition of acids such as HBr[28,51] or HI[69] can increase the solubility of inorganic compounds (here, PbX_2), supersaturation concentration, and viscosity of perovskite solutions (Figure 3b). These acids also induce an intermediate step, which retards the crystallization speed during the one-step solution process.[57]

$$PbX_2 + HX \xrightarrow{DMF} HPbX_3 \tag{5}$$

$$HPbX_3 + CH_3NH_2 \rightarrow CH_3NH_3PbX_3 \tag{6}$$
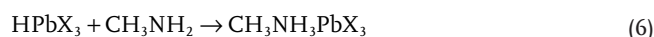
These processes retard the direct crystallization of perovskite precursors and thereby yield smooth and dense MHP PC films. An optimized concentration of HBr (6 vol%) in $MAPbBr_3$ solution has increased the average viscosity of solution from 2.5 to 3.5 mPa s, decreased the crystal size from 1.5 to 500 nm, greatly improved film uniformity, and increased the EL efficiency in PeLEDs (EQE ≈ 0.1%, CE ≈ 0.43 cd A^{-1}, L ≈ 3490 cd m^{-2}).[51] Although MHP PC film morphologies were greatly improved by adding crystallization-delaying additives, their EL efficiencies in PeLEDs were still low due to the low PLQE of MHP PC emitters arising from electron-hole pair separation into free charge carriers in the large dimension of the perovskite grain;[1,4,33] these indicate that other methods that both improve the film morphology and reduce the grain size should be developed.

2.1.3. Crystallization-Preventing Additives

In the one-step solution process, growth of perovskite crystals dominates the nucleation of crystals; thus, inhibiting growth can be a good strategy to reduce the grain size and smoothen the film.[70,71] Organic molecules mixed in perovskite solution can effectively prevent growth of perovskite crystals and induce small grains. The molecules were dissolved together in perovskite solutions, and became located between the perovskite nuclei when they were spin-coated; organic molecules reduced the space for the perovskite crystals to grow. Because the perovskite crystals grow until they meet each other or organic additive inhibitors, the presence of these organics reduce the final crystal size.[72]

Uniform and pinhole-free MHP PC films with greatly reduced grain size can be achieved by adding poly(ethylene oxide) (PEO) into the perovskite solution.[52] As the ratio of the PEO concentration to the $MAPbBr_3$ precursor concentration increased from 0.05:1 (PEO:$MAPbBr_3$) to 0.25:1, the grain size

**ADVANCED
SCIENCE NEWS**

www.advancedsciencenews.com

**small
methods**

www.small-methods.com

gradually decreased from ≈1 µm to ≈100 nm and the surface coverage increased from >80% to >95% (Figure 3c–h). These small grains can be uniformly dispersed within the composite films; broadened X-ray diffraction (XRD) peaks confirmed that these perovskite polycrystals were fairly small and randomly oriented. PEO is a good ionic conducting polymer, so addition of PEO also facilitated the migration of ionic species and induced p–i–n homojunctions in composite films. This simple method in the one-step spin-coating process was used to fabricate single-layered PeLEDs (indium tin oxide (ITO)/PEO:perovskite composite film/top electrode (In/Ga or Au)) with CE ≈ 0.74 cd A^{-1}, L ≈ 4064 cd m^{-2}, and low turn-on voltage V_{ON} ≈ 2.9 V.[52] PEO additives can also effectively reduce the grain size of all-inorganic MHPs (CsPbBr$_3$), fabricate uniform PEO:CsPbBr$_3$ composite films with pinhole-free surface coverage, and achieve high-efficiency CsPbBr$_3$ PeLEDs (EQE ≈ 4.26% and CE ≈ 15.67 cd A^{-1}[73] or EQE ≈ 4.76%, CE ≈ 21.38 cd A^{-1}, and L ≈ 51 890 cd m^{-2} after chloroform post-treatment[74]). Semiconducting poly(vinyl carbazole) (PVK)[75] and polyimide precursor dielectric (PIP)[76] have also been mixed with MAPbBr$_3$ precursors to fabricate uniform composite films and bright MAPbBr$_3$ PeLEDs (EQE ≈ 0.64%, CE ≈ 2.37 cd A^{-1}, L ≈ 1561 cd m^{-2}, V_{ON} ≈ 3.5 V in PeLEDs based on PVK:MAPbBr$_3$; EQE ≈ 1.2%, L ≈ 2800 cd m^{-1} in PeLEDs based on PIP:MAPbBr$_3$).

Mixing two organic molecules (PEO with polyvinylpyrrolidone (PVP)[77] or PVK with 1,3,5-tris(1-phenyl-1H-benzimidazol-2-yl) benzene (TPBI)[78]) can further improve the uniformity of MHP PC films, facilitate charge injection from the HIL/EML and EML/EIL interfaces due to the in situ-formed p–i–n junction in the EML[77] or efficient charge-transport properties of PVK (hole mobility ≈ 4.8 × 10^{-9} cm^2 V^{-1} s^{-1})[79] and TPBI (electron mobility ≈ 5.14 × 10^{-5} cm^2 V^{-1} s^{-1}),[80] and thus achieve an efficient EL in PeLEDs (EQE ≈ 5.7%, power efficiency PE ≈ 14.1 lm W^{-1}, L ≈ 593 178 cd m^{-2} for PeLEDs based on PEO:PVP:CsPbBr$_3$; EQE ≈ 2.28%, CE ≈ 9.45 cd A^{-1}, L ≈ 7263 cd m^{-2} for PeLEDs based on PEO:PVP:MAPbBr$_3$).

Mixing a hydrophobic polymer, poly(ethylene glycol) (PEG), scaffold with a perovskite solution also made pinhole-free and uniform MHP PC films.[81] The PEG scaffold can provide a 3D skeleton that supports the growth of perovskite crystals, improve the wettability of perovskite precursors, and decrease the crystallization rate of perovskite precursors. An excess amount of organic small molecules, 4,4-bis(N-carbazolyl)-1,1-biphenyl (CBP),[82] and inorganic salt additives, NaBr,[83] can also improve the uniformity of the MHP PC films by preventing growth of MAPbBr$_3$ crystals and by acting as a nucleation agent, respectively.

2.1.4. Multicoating

A double coating of perovskite solution (MAPbX$_3$) on top of the heated underlayers[84] and dripping a second perovskite precursor solution on the spinning perovskite quasi-film[85] can also improve the film morphology. Coating the first perovskite solution increases the wettability of the second-coated perovskite solution; this effect decreases the contact angle from 33° (on pristine poly(3,4-ethylenedioxythiophene):poly(styrenesulfonate) (PEDOT:PSS) films) to 17° (on the predeposited perovskite layer), and yields a pinhole-free morphology (>95% coverage and root-mean-square roughness r_{RMS} ≈ 1.18 nm). PeLEDs with double-coated MHP PC films showed high EL efficiencies (green emission: EQE ≈ 6.2%, CE ≈ 21 cd A^{-1}, L ≈ 16 060 cd m^{-2}; yellow emission: EQE ≈ 4.2%, CE ≈ 16 cd A^{-1}, L ≈ 4200 cd m^{-2}; red emission: EQE ≈ 5.8%, CE ≈ 19 cd A^{-1}, L ≈ 10 100 cd m^{-2}) that were much higher than in single-coated MHP PC films (green emission: EQE ≈ 1.25%; yellow emission: EQE ≈ 1%; red emission: EQE ≈ 1.23%).[84]

2.1.5. Mixing Various A-Site Cations

Mixing various organic ammoniums in the A-site in the perovskite structure can also yield uniform MHP PC films with reduced grain size. Especially, large organic ammoniums such as phenylethyl ammonium (PEA)[21,22] and 2-phenoxyethyl-amine (POEA)[86] impede the growth of MAPbX$_3$ crystals and thus reduce the grain size in the films. Furthermore, large organic ammoniums can separate 3D MHP crystals (MAPbX$_3$) by locating between PbX$_6$ octahedral planes; these form a quasi-2D structure Ruddlesden–Popper (RP), and increase E_B and PLQE by confining electron-hole pairs inside the 3D MHP crystals. Pure MAPbBr$_3$ PC films showed scattered large cubic grain with size > 1 µm, but PEA$_2$MA$_{m-1}$Pb$_m$Br$_{3m+1}$ ($m \in \{1-4\}$) films showed full film coverage with small grain size that even cannot be distinguished in scanning electron microscope images.[21] These quasi-2D MHP PC films mixed with PEA and MA showed much reduced trap density, reduced nonradiative trap-assisted recombination, and greatly increased PLQE (≈34%) compared to MAPbBr$_3$ PC films (≈2–3%), and thereby achieved higher EL efficiencies (CE ≈ 4.9 cd A^{-1}, L ≈ 2935 cd m^{-2}) than did MAPbBr$_3$ films (CE ≈ 0.082 cd A^{-1}, L ≈ 195.15 cd m^{-2}).[21] PEA$_2$(MA)$_{n-1}$Pb$_n$I$_{3n+1}$ films also showed greatly increased PLQE ≈ 27%, E_B > 200 meV, and EL efficiencies in NIR emission (EQE ≈ 8.8%, R ≈ 80 W sr^{-1} m^{-2}) in PeLEDs compared to MAPbI$_3$ films (PLQE ≈ 1%, E_B ≈ 20 meV, EQE ≈ 0.14%, R ≈ 1.2 W sr^{-1} m^{-1}).[22]

The growth of FAPbX$_3$ perovskite crystals can be also restricted by 1-naphthylmethylamine halide (NMAX) additives.[87] Quasi-2D NMA$_2$(FAPbI$_3$)$_{n-1}$PbI$_4$ films showed uniform MHP PC films with much lower r_{RMS} ≈ 2.6 nm than FAPbI$_3$ films (r_{RMS} ≈ 18.8 nm). PeLEDs with NMA$_2$(FAPbI$_3$)$_{n-1}$PbI$_4$ achieved high EL efficiency in NIR emission (EQE ≈ 11.7%, R ≈ 82 W sr^{-1} m^{-2}). NMA$_2$(FAPbI$_3$)$_{n-1}$PbI$_4$ with excellent film uniformity can also help to scale up the device area up to 64 mm^2 while maintaining high EL efficiency (EQE ≈ 7.5%). PEA can also induce uniform FAPbBr$_3$ PC films with a small grain size.[46] PEA$_2$(FAPbBr$_3$)$_{n-1}$PbBr$_4$ PC films had quasi-2D perovskite films that contained a variety of multiphases with quantum-well structures; these induced a blueshift of the PL spectrum due to the quantum-confinement effect, and high PLQE (≈57.3%) and EL efficiency in PeLEDs (EQE ≈ 14.36% by assuming the Lambertian profile of the EL emission and CE ≈ 62.43 cd A^{-1} after trioctylphosphine oxide (TOPO) treatments).[46]

Long-chain organic ammonium can also efficiently impede the growth of 3D perovskite grains, reduce grain size and surface roughness, and induce quasi-2D MHP films.[47]

Mixing *n*-butylammonium (BA) with MA reduced r_{RMS} in PC films from 3.4 nm in MAPbBr$_3$ films and 4.9 nm in MAPbI$_3$, to 1 nm in BA$_{0.2857}$MA$_{0.7143}$PbBr$_3$ films and 0.6 nm in BA$_{0.2857}$MA$_{0.7143}$PbI$_3$ films (**Figure 4**a,b). With these highly uniform quasi-2D PC films, highly efficient PeLEDs were demonstrated (EQE ≈ 10.4% in PeLEDs based on BA$_{0.17}$MA$_{0.83}$PbBr$_3$; EQE ≈ 9.3% in PeLEDs based on BA$_{0.17}$MA$_{0.83}$PbI$_3$) (Figure 4c,d). Long organic ammonium

that assembles at the surface of crystallites also impedes migration of ions and related traps, and therefore significantly improves operating stability (Figure 4e,f). These quasi-2D PC films can also change the emission wavelength (from ≈410 to ≈545 nm for Br-based MHPs[88,89] and from ≈575 to ≈760 nm for I-based MHPs,[89] respectively) by controlling the number of 3D perovskite crystal layers due to quantum-confinement effects.
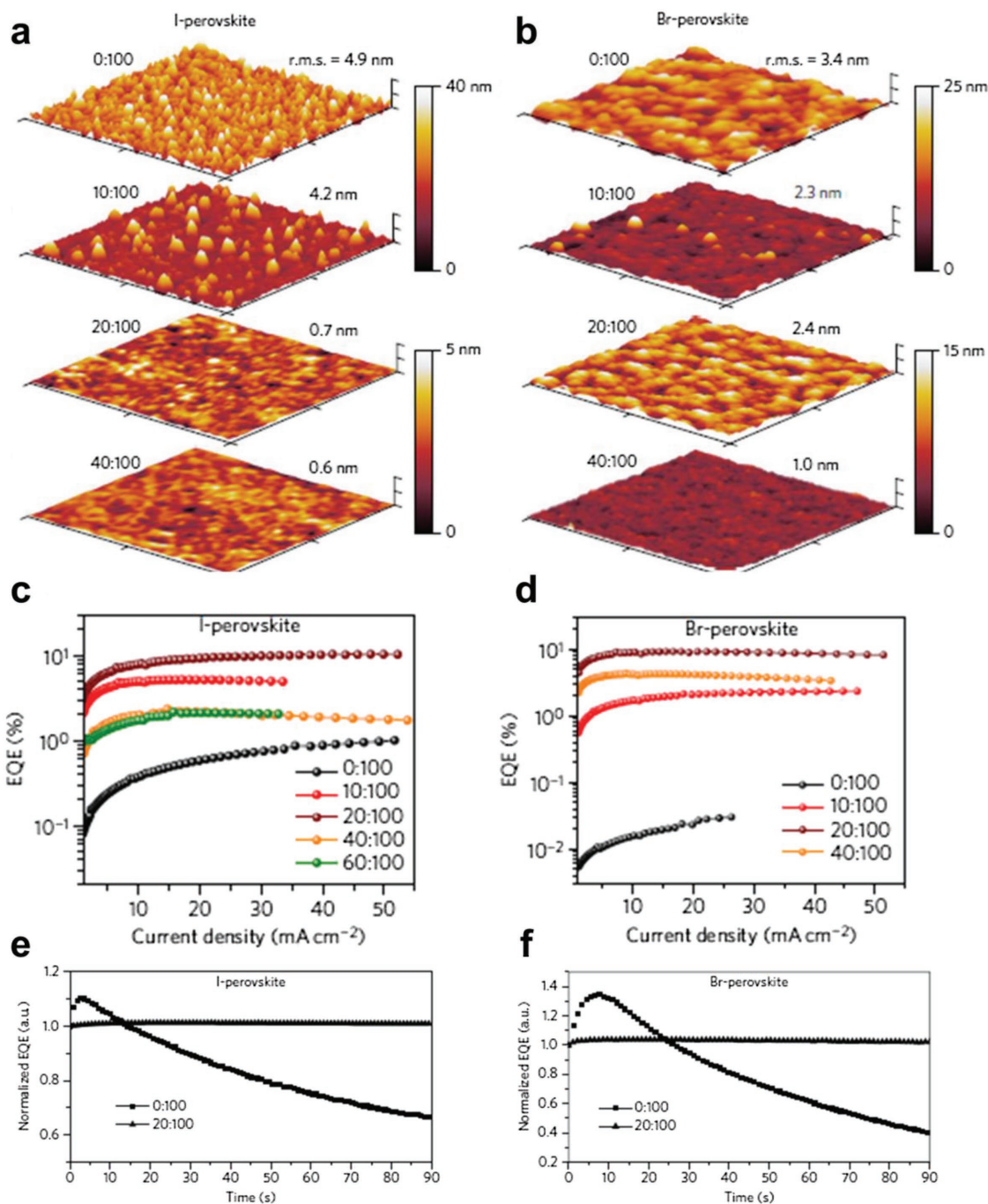
Figure 4. a,b) Atomic force microscopy images of MHP PC films with different BAI:MAPbI$_3$ ratios (a) and BABr:MAPbBr$_3$ ratios (b). c,d) EQE versus current density characteristics of PeLEDs based on PC films with different BAI:MAPbI$_3$ ratios (c) and BABr:MAPbBr$_3$ ratios (d). e,f) Operating stability of PeLEDs based on PC films with different BAI:MAPbI$_3$ ratios (e) and BABr:MAPbBr$_3$ ratios (f). Reproduced with permission.[47] Copyright 2017, Nature Publishing Group.

Mixing different small cations in the A-site of the perovskite structure can also modify the PC film morphology.[90–96] Incorporating 15% (molecular ratio) of MAPbBr$_3$ into FAPbI$_3$ stabilizes the perovskite phase of FAPbI$_3$ and induces uniform and dense morphology with improved crystallinity.[94] Adding 13% (molecular ratio) of MABr into CsPbBr$_3$ also improved the film morphology and greatly increased the EL efficiencies (EQE ≈ 10.43%, CE ≈ 33.9 cd A^{-1}, and L ≈ 91 000 cd m^{-2} in PeLEDs based on Cs$_{0.87}$MA$_{0.13}$PbBr$_3$) compared with PeLEDs based on CsPbBr$_3$ (EQE ≈ 2.41%, CE ≈ 7.19 cd A^{-1}, and L ≈ 11 600 cd m^{-2}).[93] These device efficiencies achieved by A-site engineering are the highest values[46] among the reported EL efficiencies in PeLEDs up to now; these results indicate that A-site engineering is a very effective method to enhance the EL efficiency in MHP emitters and suggests that researchers in this research field should focus more on the optimization of this A-site engineering method combined with other methods.

2.2. Two-Step Solution Process

The two-step solution process to obtain ABX$_3$ MHP PC films involves: i) depositing BX$_2$ films by spin coating BX$_2$/DMF or DMSO precursor solution, then ii) overcoating AB/isopropyl alcohol (IPA) solution on top of the BX$_2$. Nucleation rather than growth is the main crystallization mechanism in the two-step solution process, so it can be an effective method to fabricate uniform MHP PC films with small grain size, and efficient PeLEDs based on them.[97] Film morphology, grain size, and LE of MHP PC films obtained using a two-step solution process have been controlled by adjusting the concentration[98] and loading time[99] of the second deposited precursor solution, the reaction temperature,[70] and the solvent combination of the solutions that are used to fabricate the first-coated underlayers[100] or second-coated upper layers.[101]

Increasing the concentration of the MABr precursor solution from 0.18 to 0.27 M facilitated sufficient conversion of PbBr$_2$ into MAPbBr$_3$ crystals and increased the surface coverage.[98] Furthermore, increasing the concentration of the second-coated precursor solution increased the number of nuclei on the first-coated PbX$_2$ films, and thereby reduced the grain size.[102] Increasing the concentration of PbBr$_2$ from 1 to 1.5 M also yielded cubic MAPbBr$_3$ crystals with clear edges due to sufficient crystallization. Thus, MAPbBr$_3$ films converted by 1.5 M PbBr$_2$ and 0.27 M MABr precursor solutions showed a highest PLQE of 24% and the longest PL lifetime of 5.73 ns. PeLEDs based on optimized MAPbBr$_3$ films achieved EQE ≈ 0.023% and CE ≈ 0.1 cd A^{-1}, which were higher than those of PeLEDs based on other films.[98] A MAI loading time of <30 s induced insufficient conversion of PbI$_2$ to MAPbI$_3$.[99] However, a MAI loading time of >60 s induced greatly increased perovskite grain size and an excessive MAI residue on top of MAPbI$_3$ films; these traits facilitated electron-hole pair dissociation and nonradiative recombination. Therefore, the concentration and loading time of each precursor solution should be optimized to fabricate uniform and efficient MHP PC films.

FAPbBr$_3$ PC films fabricated by two-step solution processes with optimized conditions and annealing process at moderate temperature (≈70 °C) showed highly crystalline films without PbBr$_2$ spectral peaks or observable pinholes.[97] These films had average grain size (100–200 nm) and low r_{RMS} < 20 nm, and thus achieved moderate EL efficiencies (EQE ≈ 1.16%, CE ≈ 2.65 cd A^{-1}, L ≈ 13 062 cd m^{-2}) with high reproducibility. Despite the many advantages of the two-step solution process (e.g., the nucleation process as the main crystallization mechanism and the possibility of minutely controlling the reaction between precursors), EL efficiencies of MHP PC films formed by the two-step solution process are inferior than those of PC films formed by the one-step solution process.[46] Therefore, other methods such as adding additives or A-site engineering should be combined with the two-step solution process to further increase the EL efficiency.

2.3. Nanocrystal Pinning Process

Nanocrystal pinning (NCP) can efficiently reduce the grain size and induce formation of uniform MHP PC films.[4,103,104] NCP can be conducted by: i) nucleation and growth of perovskite crystals during spin coating; ii) dripping volatile solvents with high P_{vapor} on the spinning perovskite quasi-films to immediately stop the crystal growth, and thus induce uniform MHP PC films with small grains (≈100–250 nm in MAPbBr$_3$ films) (**Figure 5**a). The grain size can be further reduced by adding TPBI additives into volatile solvent (≈99.7 nm in MAPbBr$_3$ films) (Figure 5b–d).[4] MAPbBr$_3$ PC films fabricated by the NCP process based on the TPBI additive achieved a high PLQE (≈36%) and EL efficiency in PeLEDs (EQE ≈ 8.52% and CE ≈ 42.9 cd A^{-1}) (Figure 5e–g).[4] NCP can be also used to fabricate other MHP PC films[84] and in situ NC thin films (Section 4.4).[62,105]

2.4. Roll-to-Roll Process

Roll-to-roll (R2R) manufacturing methods such as blade coating,[106–111] gravure coating,[112] slot-die coating,[113,114] and spray coating[115–119] are compatible with scale up to industrial-scale production. These methods have low material waste and high throughput, and are simple and viable for large areas; these can be applied to fabricate the uniform MHP PC films and large-area PeLEDs based on them. The surface morphology of the MHP PC films printed using these R2R methods can be also modified by controlling the surface energy of the underlayer,[106] the substrate temperature,[106–109,113,115,117] the reaction atmosphere,[120] the drying airflow,[110] the composition ratio,[111] the additives,[114] the droplet sizes,[116] the coating cycle,[118] and the sequential deposition methods.[110,113]

To fabricate MHP PC films by using blade coating, perovskite solutions are loaded onto the substrate with some gap distance between the blade and the substrate (**Figure 6**a).[111] Then, the blade is dragged at a certain speed to form a meniscus of perovskite solution; the solution dries to form a film. MAPbBr$_3$:PEO composite films fabricated by the blade-coating method showed reduced grain size (≈5 µm) and improved film coverage (≈90%) (Figure 6b).[106,111] PeLEDs with simplified structure, in which both MAPbBr$_3$:PEO composite films and silver-nanowire electrodes were fabricated by blade coating in air,
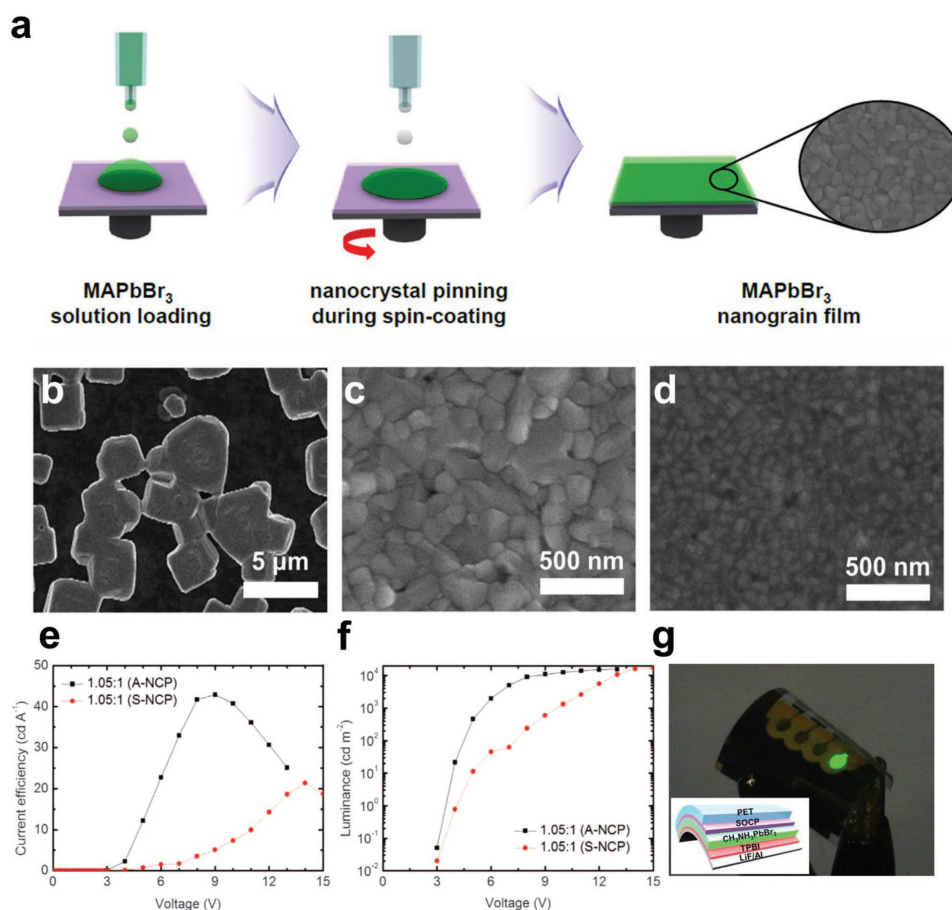
**ADVANCED
SCIENCE NEWS**

www.advancedsciencenews.com

**small
methods**

www.small-methods.com

Figure 5. a) Schematic illustration of NCP process. b–d) SEM images of MAPbBr$_3$ PC films without NCP process (b), with NCP process (c), and with a TPBI additive–based NCP process (d). e–g) Current efficiency versus voltage characteristics (e), luminance versus voltage characteristics (f), and operating image (g) of PeLEDs. Reproduced with permission.[4] Copyright 2015, American Association for the Advancement of Science.

achieved EQE ≈ 1.1%, CE ≈ 4.91 cd A^{-1}, and L ≈ 21 014 cd m^{-2} (Figure 6c,d).[111] These printing methods can also fabricate flexible PeLEDs (EQE ≈ 0.14%, CE ≈ 0.6 cd A^{-1}, L ≈ 360 cd m^{-2}) on polymer substrates/carbon nanotube electrodes.[111]

3. Vacuum-Deposited Polycrystalline Bulk Films and Light-Emitting Diodes

The vacuum deposition process can be used to fabricate MHP PC bulk films and PeLEDs. This method has various advantages, such as small batch-to-batch variation, easy patterning, and insensitivity to environmental atmosphere. Under gradual heating in a high vacuum, each perovskite precursor evaporates and diffuses; they reassemble on the target substrate and assemble into perovskite crystals.[121,122] Vacuum deposition does not require consideration of the physical properties of the underlayers or the choice of appropriate solvents to dissolve the perovskite precursors; therefore, this method is more easily adapted to demonstrate multilayered and tandem PeLEDs than the solution process. Furthermore, vapor-deposited MHP PC films do not have imperfections or impurities such as a solvation intermediate phase (perovskite-solvent) that occurs in solution-processed PC films due to the in

situ growth of perovskite crystals and interactions with solvents.[40,121,122]

In this section, we review recently reported publications about vapor deposition of MHP PC films and their application on PeLEDs. We categorize these technologies in detail: i) coevaporation deposition;[35–39] ii) sequential deposition;[123–126] iii) flash evaporation;[127–130] iv) chemical vapor deposition (CVD);[131–135] v) VASP.[40–42]

3.1. Coevaporation Deposition

Coevaporation deposition methods use separate sources because two precursors for fabricating perovskite crystals have different deposition temperature (e.g., ≈70 °C[136] or ≈100 °C[137] for MAI and ≈250–280 °C for PbI$_2$[136,137]) (**Figure 7**a). Vapor-phase perovskite precursors meet and react to fabricate perovskite crystals on the target substrate. MHP PC films deposited by coevaporation showed highly uniform and flat films over scales of tens of micrometers, whereas solution-processed MHP PC films showed nonuniform film morphologies with varying thicknesses and pinholes.[35] These uniform films showed excellent reproducibility with finely controllable thickness and reaction precursor ratio,[37,38] and can be used in
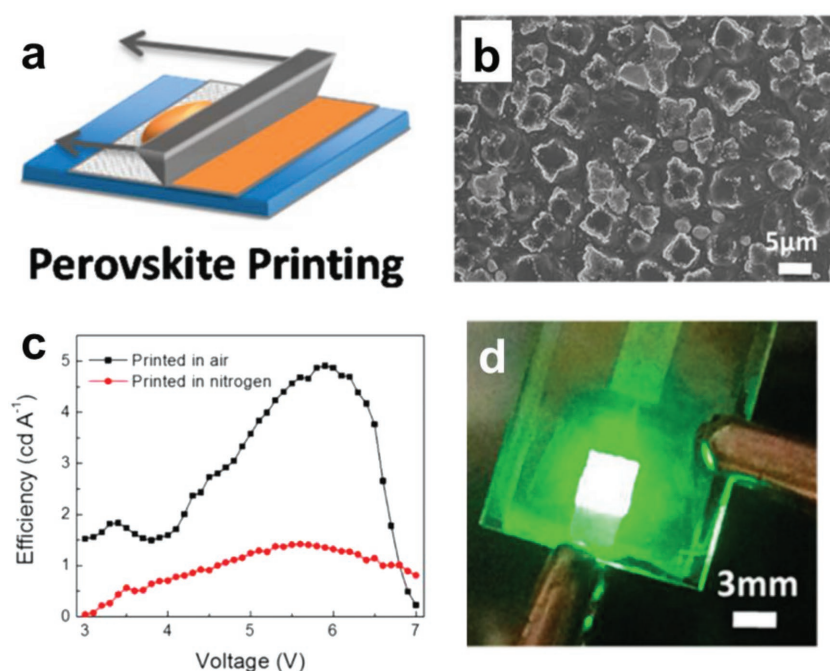
**ADVANCED
SCIENCE NEWS**

www.advancedsciencenews.com

**small
methods**

www.small-methods.com

Figure 6. a) Schematic illustration of the blade coating process of MHP PC bulk films. b–d) SEM image of MAPbBr$_3$:PEO composite films (b), current efficiency versus voltage characteristics (c), and photograph (d) of operating PeLEDs based on blade-coated MAPbBr$_3$:PEO composite films. Reproduced with permission.[111] Copyright 2015, American Chemical Society.

PeLEDs.[39] Reported PeLEDs with MAPbBr$_3$ PC films deposited by coevaporation achieved EQE = 0.06%.[36] EL and PL spectra, atomic compositions, and film morphologies of these coevaporation-deposited MHP PC films can also be modified by sequential deposition of different perovskite moieties.[36]

Even though coevaporation-deposited MHP PC films show a highly uniform film morphology, they show inferior EL efficiencies than solution-processed MHP PC films.[46] Here, we categorize the possible reasons: i) the perovskite precursors (e.g., MAI, MABr, MACl) can diffuse freely and undirectionally in the vacuum chamber due to their small molecular weight and can interfere with the monitoring of the deposition rate of other precursors (e.g., PbI, PbBr, PbCl);[123] ii) the high reaction rate between the MAX and the PbX$_2$ in the coevaporation method can leave unreacted precursors in the PC films, which induce nonstoichiometry in MHP PC films and limit the LE in them; iii) one precursor can contaminate the other precursor that is contained in the other crucible; iv) predeposited perovskite precursors on the wall inside the chamber can be desorbed and contaminate the samples. Furthermore, other reports in the literature only used organic–inorganic MHPs (e.g., MAPbBr$_3$, MAPbI$_3$) which had volatile components due to low deposition temperature ($\approx$70 °C[136] or $\approx$100 °C[137] for MAI and $\approx$150–175 °C[127] for MABr); these can also induce the easy undirectional diffusion of molecules in the chamber and hinder the formation of highly crystalline MHP PC films. Therefore, MHP PC films with components that have a high decomposition temperature (e.g., CsPbBr$_3$ has decomposition temperature of 580 °C[138]) should be fabricated for efficient PeLEDs.

3.2. Sequential Vapor Deposition

Layer-by-layer sequential vapor deposition methods sublimate MAX precursors onto predeposited PbX films, where it crystallizes (Figure 7b). This method avoids the problems of the coevaporation methods that were discussed in Section 3.1. The reaction depth and rate between the deposited PbX and MAX can be controlled by tuning the substrate temperature.[123] The thickness and characteristics of the devices that use them can be modified by varying the PbX/MAX deposition cycles[124] or MAX deposition duration.[125] MHP PC films with mixed A-site can be fabricated using sequential vapor deposition by premixing A-site precursors in the crucible; the PL emission wavelength and the crystal composition of the (PEA)$_2$(MAPbBr$_3$)$_n$PbBr$_4$ films can be controlled by tuning the ratio of MABr to phenethylammonium bromide (PEABr).[126] (PEA)$_2$(MAPbBr$_3$)$_n$PbBr$_4$ films with optimized MABr:PEABr ratio (1:0.25) showed higher EL efficiencies in PeLEDs (EQE $\approx$ 0.36%, CE $\approx$ 1.3 cd A^{-1}) than films with other MABr:PEABr ratio (EQE $\approx$ 0.00061%, CE $\approx$ 0.002 cd A^{-1} for 1:0 ratio and EQE $\approx$ 0.0059%, CE $\approx$ 0.02 cd A^{-1} for a 1:0.5 ratio). MHP PC films fabricated by sequential vapor deposition methods showed very narrow emission linewidth (18.6 nm) with Commission Internationale d'Eclairage coordinates of (0.2, 0.75), which correspond to highly saturated green.[2,126]

3.3. Flash Evaporation

Flash evaporation may be an alternative method to deposit MHP PC films.[129,130] First, a tantalum (Ta) heater foil is precoated with perovskite material by a solution process, then a strong current is passed through the foil to induce evaporation of the perovskite crystals (Figure 7c). Because the perovskite crystals have already been formed, the temperature of the Ta foil can be lower than that of the crucible that is used in the coevaporation and sequential vapor deposition methods;[127,128] this reduction in temperature can prevent the decomposition of organic compounds, which can occur as[127,128]

$$CH_2NH_3Br \rightarrow CH_2NH_2 + HBr \qquad (7)$$
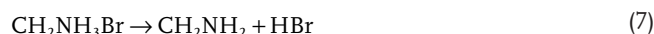
This method can fabricate 3D, layered, and 2D MHP PC films with different ammonium cations at the A-site,[130] and thus can be successfully applied to PeLEDs.

3.4. Chemical Vapor Deposition

The CVD process can be used in a variety of industrial processes because CVD methods need only moderate vacuum

**ADVANCED
SCIENCE NEWS**

www.advancedsciencenews.com
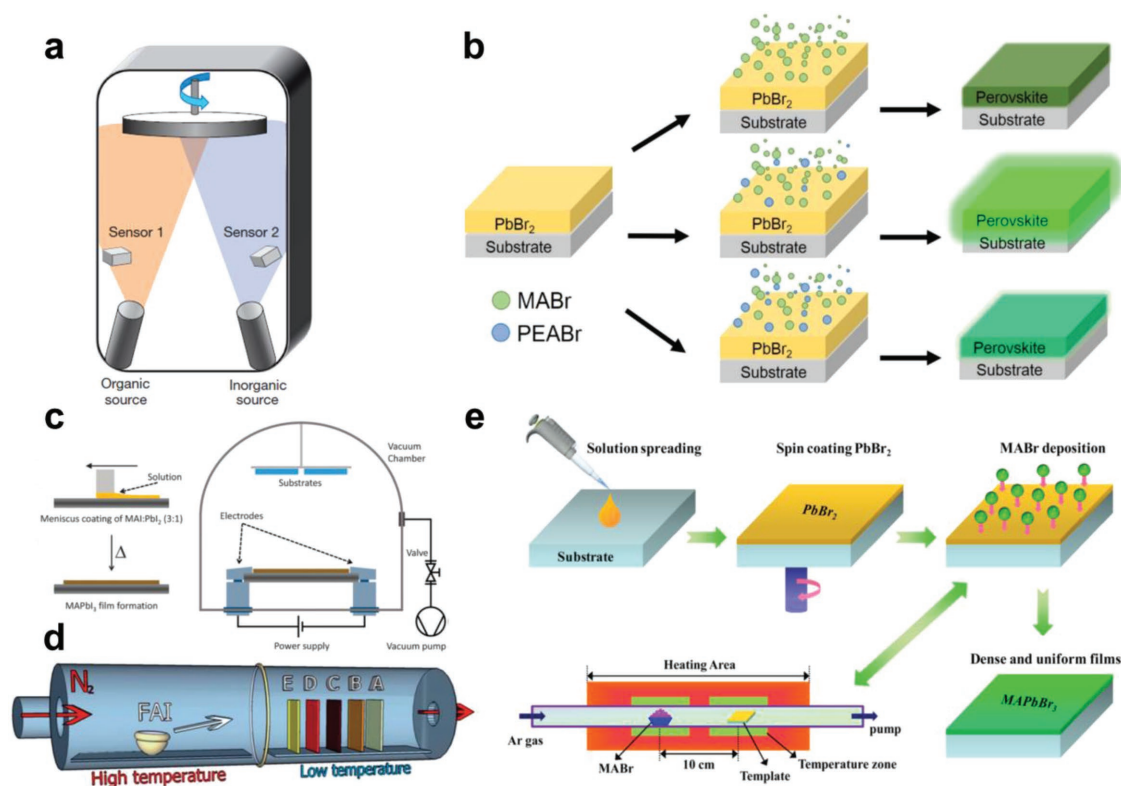
**small
methods**

www.small-methods.com

Figure 7. a–e) Schematic illustrations of the coevaporation deposition method (a), sequential the vapor deposition method (b), flash evaporation (c), chemical vapor deposition (d), and VASP (e) for MHP PC bulk films. (a) Reproduced with permission.[35] Copyright 2013, Nature Publishing Group. (b) Reproduced with permission.[126] Copyright 2017, American Chemical Society. (c) Reproduced with permission.[129] Copyright 2015, the Royal Society of Chemistry. (d) Reproduced with permission.[139] Copyright 2014, the Royal Society of Chemistry. (e) Reproduced with permission.[41] Copyright 2017, American Chemical Society.

pressure ($\approx 10^{-3}$ Pa), are compatible with large-area processes, and have excellent sample-to-sample variation.[131–133,139] For the formation of MHP PC films, CVD methods have advantages such as: i) no need for additional postannealing process because perovskite crystal grows at high temperature, and ii) possible controllability of gas flow, which affects the reaction rate of the perovskite crystal uniformity (Figure 7d).[131–133,139] Furthermore, high-quality MHP PC films can be formed in a low-pressure atmosphere[134] and even under ambient pressure by aerosol-assisted CVD methods.[135] The perovskite grain size can be further controlled by tuning the substrate temperatures T_S; the perovskite grain size increased with increasing T_S; optimized MHP PC films achieved maximum EQE $\approx 0.02\%$, CE ≈ 0.06 cd A^{-1}, and $L \approx 900$ cd m^{-2} in PeLEDs.[132] These EL efficiencies are still low. Inspired by the one-step solution-processed MHP PC films, we suggest that codeposition of organic semiconductors with precursors or diverse A-site organic ammonium cations can further improve the EL efficiencies in PeLEDs.
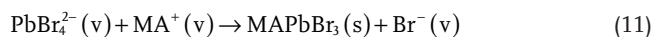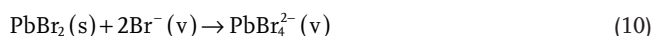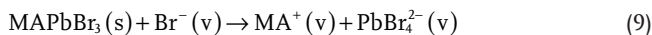
3.5. Vapor-Assisted Solution Process

Vacuum-deposition methods can be combined with solution-process methods to fabricate uniform MHP PC films; this method is called the VASP.[40–42] Generally, VASP methods

include two sequential steps: i) fabricating PbX$_2$ solid films by a solution process, such as spin coating; ii) depositing MAX vapor on predeposited PbX$_2$ films and inducing gas–solid crystallization process uniformity (Figure 7e).[41]

$$PbBr_2(s) + MA^+(v) + Br^-(v) \rightarrow MAPbBr_3(s) \tag{8}$$

MHP PC films fabricated by gas–solid crystallization avoid the perovskite–solvent complexes that arise in the solution-process method.[40] In the VASP method, a dissolution–recrystallization growth mechanism may occur: under Br vapor, MAPbBr$_3$ crystals or PbBr$_2$ films were redissolved into ions, and then recrystallized as[41]

$$MAPbBr_3(s) + Br^-(v) \rightarrow MA^+(v) + PbBr_4^{2-}(v) \tag{9}$$

$$PbBr_2(s) + 2Br^-(v) \rightarrow PbBr_4^{2-}(v) \tag{10}$$

$$PbBr_4^{2-}(v) + MA^+(v) \rightarrow MAPbBr_3(s) + Br^-(v) \tag{11}$$

as the MABr concentration and deposition duration increased; the remaining underlying PbBr$_2$ layer converted to MAPbBr$_3$ crystals and the surface coverage increased. Increasing the evaporation temperature of MABr powders also facilitates crystallization and yields uniform films. PeLEDs based on
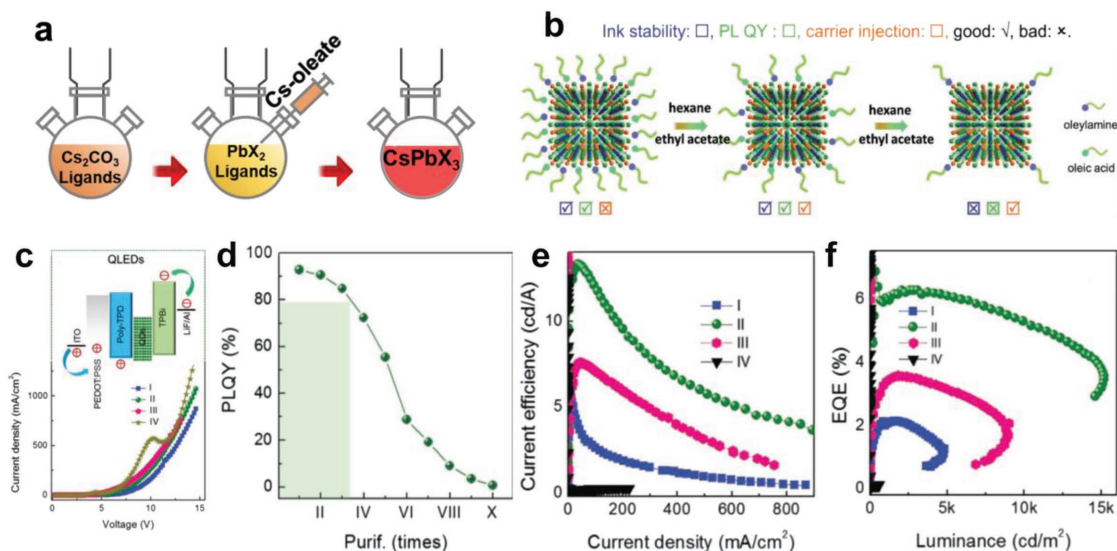
Figure 8. a,b) Schematic illustrations of the hot-injection method (a), and ligand density control of colloidal MHP NCs (b). c) Current density versus voltage characteristics of PeLEDs based on MHP NCs with different purification cycles. d) PLQE of MHP NCs with different purification cycles. e,f) Current efficiency versus voltage characteristics (e) and EQE versus voltage characteristics (f) of PeLEDs based on MHP NCs with different purification cycles. Reproduced with permission.[158] Copyright 2016, Wiley-VCH.

MAPbBr$_3$ PC films with optimized fabrication conditions (deposition duration ≈ 25 min, MABr power temperature ≈ 180 °C) showed maximum EQE ≈ 4.36%, CE ≈ 8.16 cd A^{-1}, and L ≈ 6530 cd m^{-2}.[41]

4. Colloidal Nanocrystals and Light-Emitting Diodes

MHP NCs with size of less than a few tens of nanometers have high PLQE (90%) and even can be easily synthesized at room temperature in air conditions, maintaining excellent optical properties; these various advantages make them promising emitters in PeLEDs and competitive with conventional inorganic QDs and QD LEDs.
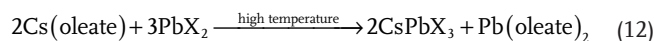
4.1. Template-Assisted Growth

Noncolloidal MHP NCs without ligands were synthesized by depositing perovskite solution on preheated mesoporous Al$_2$O$_3$ films.[140] As the solvents evaporated, the perovskite precursors crystallized in the porous matrixes; these MHP NCs have PLQE of >50% even though they have no surface ligands.[141] The NC size and PL spectrum of template-assisted-grown NCs can be tuned by controlling the pore size of the template.[142]

4.2. Hot-Injection Methods

Hot injection is the best-known method to synthesize colloidal semiconductor NCs or QDs, and it can be used to synthesize monodispersed MHP NCs. Generally, PbX$_2$ precursors are dissolved in a hot hydrophobic solvent (octadecene (ODE)) which predissolves the acid ligands and amine ligands; Cs precursors

(e.g., Cs$_2$CO$_3$) are dissolved in a separate hot solvent with acid ligands, which make Cs-oleate in N$_2$ or Ar inert atmosphere (**Figure 8**a).[143] When the Cs-oleate is injected into the PbX$_2$ solution, MHP NCs can be synthesized as[143]

$$2\text{Cs}(\text{oleate}) + 3\text{PbX}_2 \xrightarrow{\text{high temperature}} 2\text{CsPbX}_3 + \text{Pb}(\text{oleate})_2 \quad (12)$$

These MHP NCs have very high PLQE (recently, MHP NCs with PLQE ≈ 100% have been reported[34,144]) and high color purity with narrow emission linewidth (FWHM < 20 nm).[143] The size, shape, and emission wavelength can be controlled by tuning the reaction temperature and reaction time. 2D nanoplates and 1D nanowires can be formed by ligand engineering,[145–147] reaction-temperature engineering,[146] purification,[148] ultrasonication,[149] A-site-cation engineering,[150] or by using additives.[151] Furthermore, the synthesized MHP NCs can be also post-transformed from 3 nm thick CsPbBr$_3$ nanosheets to Pb nanoparticle (NP)–CsPbBr$_3$ nanocomposites by electron beams,[152] from 2D CsPbBr$_3$ nanoplatelets to larger structures such as nanobelts or square-shaped nanodisks by photoirradiation,[153,154] or from cubic phase to orthorhombic phase in FAPbBr$_3$ crystals by pressure.[155]

The first PeLEDs based on MHP NCs synthesized by hot-injection methods showed relatively low EL (blue emission: EQE ≈ 0.07%, CE ≈ 0.14 cd A^{-1}, L ≈ 742 cd m^{-2}; green emission: EQE ≈ 0.12%, CE ≈ 0.43 cd A^{-1}, L ≈ 946 cd m^{-2}; orange emission: EQE ≈ 0.09%, CE ≈ 0.08 cd A^{-1}, L ≈ 528 cd m^{-2}).[156] These low ELs are due to the insulating ligands, which impede charge transport in the NP films; therefore, many researchers have tried to increase the EL efficiencies of MHP NCs by ligand engineering.

Replacing the long ligands (oleic acid and oleylamine) with relatively short ligands (didodecyldimethylammonium bromide (DDAB)) was found to improve charge transport in the NC films and increased the EL efficiencies (blue emission: EQE ≈ 1.9%, L ≈ 35 cd m^{-2}; green emission: EQE ≈ 3%, L ≈ 330 cd m^{-2}).[157]

ADVANCED
SCIENCE NEWS
www.advancedsciencenews.com

small
methods
www.small-methods.com

Purification by washing the NCs with hexane/ethyl acetate solvent mixtures can effectively reduce the surface ligand density and improve the charge-transport properties (Figure 8b,c).[158] However, purification for more than four cycles has seriously degraded the stability and PLQE of MHP NCs (Figure 8d). PeLEDs with MHP NCs that had been washed three times showed much improved EL efficiencies (EQE ≈ 6.27%, CE ≈ 13.3 cd A^{-1}, L ≈ 15 185 cd m^{-2}) (Figure 8e,f).[158] Recently, by performing both ligand exchange and purification, a high EQE of 8.73% and CE of 18.8 cd A^{-1} were achieved in green-emitting PeLEDs based on MHP NCs synthesized by hot injection.[48]

4.3. Recrystallization Methods

Recrystallization methods that can be performed in air at room temperature have been developed to overcome the disadvantages of hot-injection methods, such as the complex synthesis process and the high synthesis cost.[159,160] First, perovskite precursors were dissolved in polar solvents such as DMF and DMSO. These perovskite solutions were dripped into less-polar solvents such as toluene; the solubility of the perovskite precursors suddenly decreased in the mixed solvent, so they were crystallized (**Figure 9**a). If perovskite solutions were dripped into unmixable less-polar solvents such as hexane, they formed emulsion states, then were crystallized by mixing with a demulsifier (e.g., *tert*-butanol).[14,161] Then, the premixed organic ligands adhered to the surface of the MHP NCs and prevented the aggregation of the NCs in colloidal solution.[160] MHP NCs synthesized by recrystallization methods have shown similar LE and photostability to those synthesized by hot-injection methods.[159] The size and shape of MHP NCs can be controlled

by tuning the synthesis temperature,[162] A-site cations,[163] ligand density,[13] and ligand length.[14,146] This method also allows the use of crosslinkable and polymerizable ligands to increase the moisture stability of the MHP NCs.[164]

As ligand density and length decrease, the size of the MAPbBr$_3$ and FAPbBr$_3$ NCs increases gradually (Figure 9b).[13,14] MHP NCs with particle size >D_B showed improved PLQE because the low surface-to-volume ratio reduced the number of surface defects, and the decreased ligand density and length improved the charge-transport characteristics in the film states (Figure 9c,d). PeLEDs based on MAPbBr$_3$ and FAPbBr$_3$ NCs with dimension >D_B achieved high CE ≈ 15.5 cd A^{-1} (Figure 9e)[13] and CE ≈ 9.16 cd A^{-1}.[14] Mixing FAPbBr$_3$ 2D nanoplatelets with polymer matrixes also achieved high EL efficiencies (CE ≈ 13.02 cd A^{-1}).[165] Although MHP NCs showed higher PLQE than MHP PC films, they showed lower EL efficiencies than MHP PC films[46] due to remaining insulating organic ligands and aggregation problems during the film formation process.

4.4. In Situ Formation

MHP NCs grown in situ are formed during film formation and do not need organic ligands; this process avoids the problems of colloidal NCs such as aggregation of NCs in high-concentration solutions and during film formation,[166] and impedes charge transport by insulating ligands.[48,157,158] MHP NCs can be fabricated in situ by combining A-site engineering methods (Section 2.3) and NCP methods (Section 2.3). The growth of perovskite crystals can be efficiently suppressed by dripping toluene onto spinning perovskite quasifilms
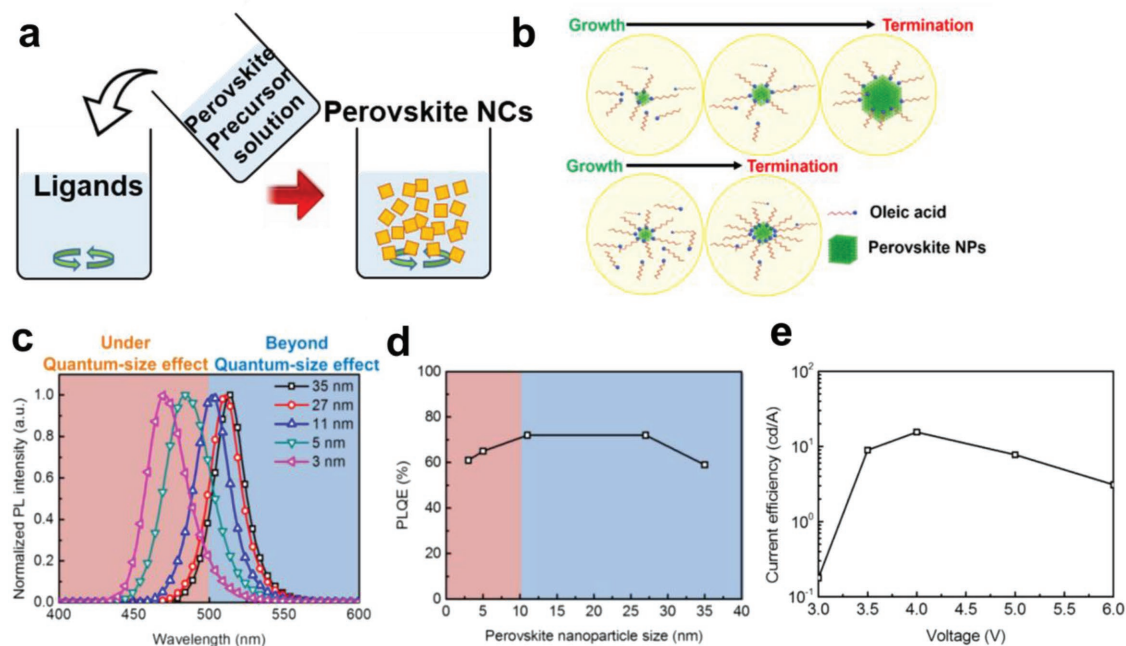

Figure 9. a,b) Schematic illustrations of recrystallization methods (a) and size control of colloidal MHP NCs (b). c,d) PL spectrum (c) and PLQE (d) of colloidal MHP NCs with different sizes. e) Current efficiency versus voltage characteristic of PeLEDs based on MHP NCs synthesized by recrystallization methods. Reproduced with permission.[13] Copyright 2017, American Chemical Society.

**ADVANCED
SCIENCE NEWS**

www.advancedsciencenews.com

**small
methods**

www.small-methods.com

that contain both perovskite precursors (MABr, PbBr$_2$, MAI, PbI$_2$) and bulky organic ammonium halide additives (PEABr, 4-fluorophenylmethylammonium iodide (FPMAI)); as a result, NCs of size < 10 nm were formed in matrix films.[105] The NCP process without bulky organic ammonium halide additives yields MHP PC films rather than NC-in-matrix films. MHP NCs grown in situ showed a blueshifted PL, possibly due to increased disorder or the quantum-confinement effect. They also showed increased PL lifetime because bulky organic ammonium additives passivated the surface trap states and reduced nonradiative recombination.[105] MHP NCs grown in situ achieved much higher PLQE (≈10.9% for MAPbBr$_3$ NCs) and EL efficiencies in PeLEDs (EQE ≈ 7.9% in MAPbI$_3$ and EQE ≈ 7% in MAPbBr$_3$ NCs) compared with MHP PC films that were fabricated without additives (PLQE ≈ 0.4% in MAPbBr$_3$ PC films; EQE ≈ 0.2% in MAPbI$_3$ and EQE ≈ 0.3% in MAPbBr$_3$ PC films).[105] MHP NCs grown in situ also improved the operating stability of PeLEDs because the bulky organic ammonium additives covered the grain boundaries and impeded ion migration. Excess amounts of MABr in perovskite precursors also suppress the crystal growth and thus achieve in situ-grown MAPbBr$_3$ NC films and high EL efficiencies in PeLEDs (EQE ≈ 8.21%, CE ≈ 34.46 cd A^{-1}).[62]

4.5. Microwave-, Sonication-, or Milling-Assisted Crystallization

Microwave irradiation[43,167] and sonication[44,168,169] have been also reported as good one-pot synthesis methods to provide colloidal MHP NCs with high product yields, good reproducibility, compatibility with mass production, and easily tunable optophysical and morphological properties (**Figure 10**a,b). MHP NCs can be synthesized by mixing organic ligands (e.g., oleic acid, oleylamine) and perovskite precursors (e.g., Cs$_2$CO$_3$, PbX$_2$) in a hydrophobic solvent (e.g., ODE); then,

under microwave irradiation or sonication, solid precursors dissolve near the liquid–solid interface; the dissolved perovskite precursors react with each other to nucleate the crystal seeds; then, they grow under continuous microwave irradiation.[43,167,168] The duration of the microwave irradiation strongly affects the size and shape of the MHP NCs; NCs were found to grow from ≈5 to ≈15 nm during the first 15 min of microwave irradiation, but irradiation > 15 min can destroy NCs by excessive energy[43] or transform them from nanocubes to nanowires.[167] Diverse shapes of NCs such as nanorods, nanowires, nanoplates, and nanocubes can be achieved by controlling the concentration of the perovskite precursors or ligands, by predissolving the precursors before reaction, and by heating the reaction solution.[43,167] A high synthesis temperature (>180 °C) and slow heating rates (<8 °C min^{-1}) during MHP NC synthesis by microwave irradiation can weaken the bonds between the organic ligands and the NC surface, and thereby induce agglomerated and nonuniform NCs.[167]

Solvent-free mechanical milling/grinding at room temperature can also crystallize perovskite precursors (e.g., CsX and PbX$_2$) into perovskites by inducing heating/supplying reaction energy, as microwave irradiation and sonication methods do (Figure 10c).[45] This reaction also occurs in three steps: each precursor is changed to an amorphous solid under mechanical milling/grinding; then chemical reactions such as nucleation and growth of amorphous perovskite crystals occur; then perovskite crystals form and unreacted precursors are exposed to further crystallization cycles. The LE of NCs was greatly increased by adding amine ligands. The shapes and sizes of the NPs were controlled by the milling speed and duration. These MHP NCs showed easy color tunability (400 < λ < 700 nm) and high PLQE (≈90% for NCs synthesized by microwave-irradiation methods,[43] ≈72% for NCs by sonication methods,[44] and ≈44% for NCs by milling/grinding method[45]), so they can be applied on efficient PeLEDs.

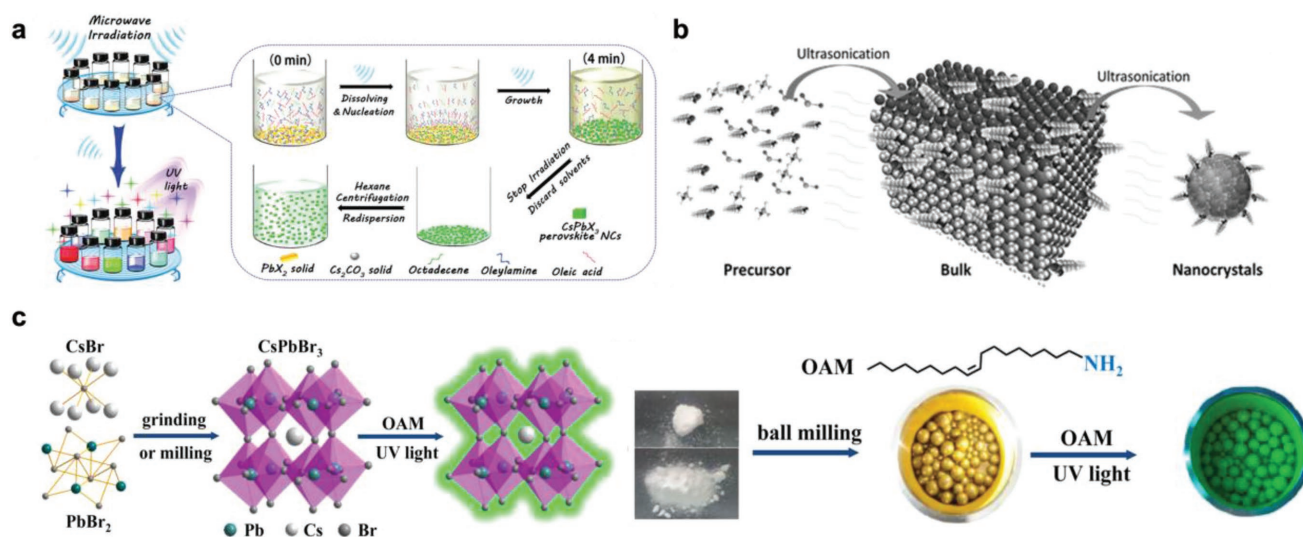**Figure 10.** a–c) Schematic illustrations of microwave-assisted crystallization (a), sonication-assisted crystallization (b), and milling-assisted crystallization (c) of MHP NCs. (a) Reproduced with permission.[43] Copyright 2017, the Royal Society of Chemistry. (b) Reproduced with permission.[44] Copyright 2017, Wiley-VCH. (c) Reproduced with permission.[45] Copyright 2017, American Chemical Society.

**ADVANCED
SCIENCE NEWS**
www.advancedsciencenews.com

**small
methods**
www.small-methods.com

5. Single Crystals and Light-Emitting Diodes

MHP SCs that do not have grain boundaries inside their crystals have fewer defect states than MHP PCs or NCs.[170–172] Therefore, we have categorized PeLEDs based on MHP SCs as PeLEDs that do not have any grain boundaries inside their emitting MHP crystals. PeLEDs based on MHP films that consist of lots of micro- or nanocrystals have been categorized as PeLEDs based on PC films or NC films and are discussed in the previous sections because those had lots of grain boundaries inside their emitting MHP films. Furthermore, MHP SCs that lack grain boundaries enable researchers to study the optical and electrical properties of pure MHPs excluding the effects of grain boundaries,[173–175] and to correlate these properties with device efficiency in PeLEDs.[176] The possibility of controlling the size from a few centimeters to a few nanometers, and the dimensionality from 3D to 2D microdisks, nanosheets, nanoplatelets, and 1D nanowires can enable MHP SCs to be used as emitters in PeLEDs.

5.1. Top-Seeded Solution Growth

High-quality MHP SCs with large size of >1 mm can be synthesized by the top-seeded solution-growth (TSSG) method.[170] In this method, small MHP SCs are placed on the bottom of a bottle that is maintained at 75 °C; a Si substrate is placed on the upper side of the bottle and kept at less than 75 °C (**Figure 11**a). Small MHP SCs sublimate under the high temperature and renucleate on the Si substrate, then grow for several days. MAPbI$_3$ SCs synthesized by TSSG methods had a trap density of 3.6×10^{10} cm^{-3}, which is five orders of magnitude lower than that in MAPbI$_3$ PCs (2.0×10^{15} cm^{-3}).[170] Other perovskite materials such as MASnI$_3$ and FASnI$_3$ can be also synthesized by TSSG.[171,172]

5.2. Bottom-Seeded Solution Growth

MHP SCs can be also synthesized by the bottom-seeded solution growth (BSSG) method.[177,178] In this method, the seed crystal is placed at the middle of a designed tray that can be rotated by an electric motor, then the saturated solution is slowly cooled down (Figure 11b). Nucleation and growth of the seed crystals occur by spontaneous crystallization. With this method, Pb-free SCs (e.g., NH(CH$_3$)$_3$SnCl$_3$, NH(CH$_3$)$_3$SnCl$_3$) can be synthesized.[179]

5.3. Antisolvent Vapor Crystallization

Antisolvent vapor crystallization (AVC) is very effective method to grow large MHP SCs >100 mm^3.[180] By slowly diffusing an
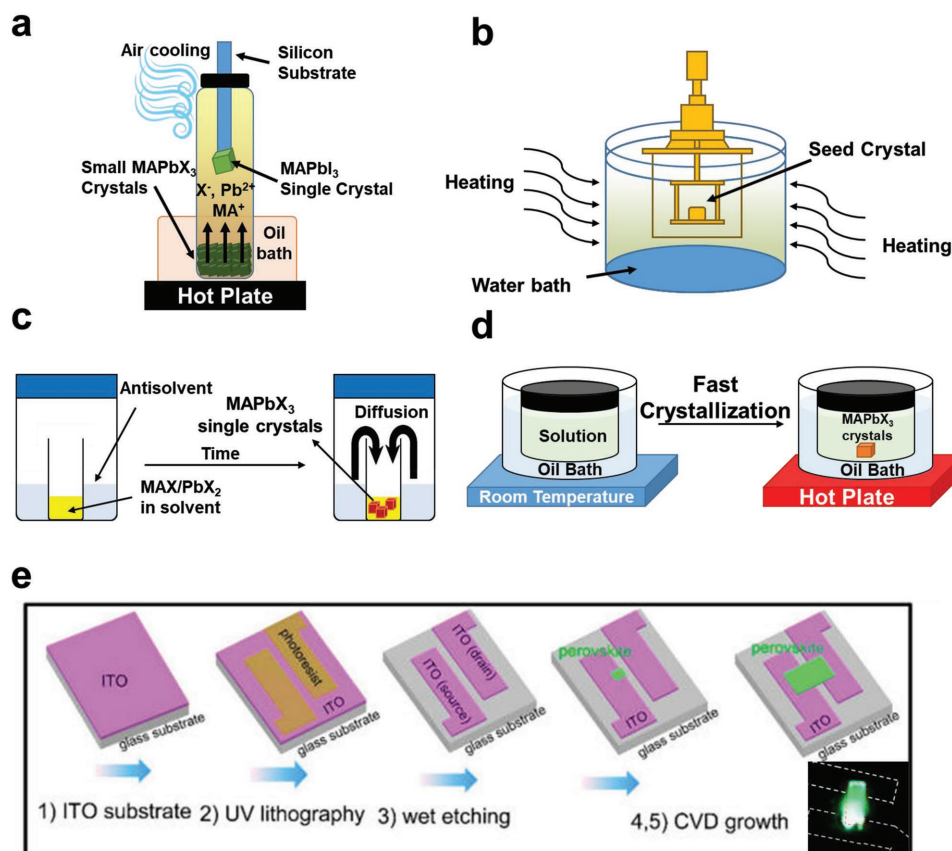
Figure 11. a–d) Schematic illustrations of top-seeded solution growth (a), bottom-seeded solution growth (b), antisolvent vapor crystallization (c), and inverse temperature crystallization (d). e) Schematic illustrations describing the fabrication process of PeLEDs based on MHP SCs synthesized by the CVD-growth method. The inset is a photograph of an operating PeLED. Reproduced with permission.[49] Copyright 2017, American Chemical Society.

Table 1. Reported EL efficiencies of PeLEDs based on various MHP crystal forms.

Crystal forms	Publication date[ref]	Crystallization method	Emission layer	Device structure	EL efficiencies
Solution-processed PC bulk films	2014/04[3]	One-step solution process	$MAPbBr_3$ $MAPbI_{3-x}Cl_x$	ITO/PEDOT:PSS/MAPbBr₃/F8/Ca/Ag ITO/TiO₂/MAPbI₃₋ₓClₓ /F8/MoO₃/Ag	EQE ≈ 0.1%, CE ≈ 0.3 cd A⁻¹, L ≈ 364 cd m⁻² EQE ≈ 0.76%, radiance ≈ 13.2 W sr⁻¹ m⁻²
	2014/11[2]		$MAPbBr_3$	ITO/buffer HIL/MAPbBr₃/TPBI/LiF/Al	EQE ≈ 0.125%, CE ≈ 0.577 cd A⁻¹, L ≈ 417 cd m⁻²
	2015/11[51]	With crystallization-delaying additives	$MAPbBr_3$	ITO/PEDOT:PSS/MAPbBr₃/SPB-02T/LiF/Ag	EQE ≈ 0.1%, CE ≈ 0.43 cd A⁻¹, L ≈ 3490 cd m⁻²
	2015/08[52]		$MAPbBr_3$:PEO	ITO/ MAPbBr₃:PEO/In/Ga	EQE ≈ 0.165%, CE ≈ 0.74 cd A⁻¹, L ≈ 4064 cd m⁻²
	2016/08[73]		$CsPbBr_3$:PEO	ITO/PEDOT:PSS/ CsPbBr₃:PEO/TPBI/LiF/Al	EQE ≈ 4.26%, CE ≈ 15.67 cd A⁻¹, L ≈ 53 525 cd m⁻²
	2017/05[74]		$CsPbBr_3$:PEO	ITO/PEDOT:PSS/ CsPbBr₃:PEO/TPBI/LiF/Al	EQE ≈ 4.76%, CE ≈ 21.38 cd A⁻¹, L ≈ 51 890 cd m⁻²
	2015/02[76]		$MAPbBr_3$:PIP	ITO/PEDOT:PSS/MAsPbBr₃:PEO/F8/Ca/Ag	EQE ≈ 1.2%, L ≈ 2800 cd m⁻²
	2016/12[77]		$CsPbBr_3$:PEO:PVP	ITO/CsPbBr₃:PEO:PVP/In/Ga	EQE ≈ 5.7%, PE ≈ 14.1 lm W⁻¹, L ≈ 593 178 cd m⁻²
	2017/03[84]	Multicoating	$MAPbI_{3-x}Br_x$	ITO/PEDOT:PSS/MAPbI₃₋ₓBrₓ/ Ca:ZnO/Ca/Al	Green: EQE ≈ 6.2%, CE ≈ 21 cd A⁻¹, L ≈ 16 060 cd m⁻² Yellow: EQE ≈ 4.2%, CE ≈ 16 cd A⁻¹, L ≈ 4200 cd m⁻² Red: EQE ≈ 5.8%, CE ≈ 19 cd A⁻¹, L ≈ 10 100 cd m⁻²
	2016/06[21]	With A-site engineering	$PEA_2(MA)_{n-1}Pb_nBr_{3n+1}$	ITO/buffer HIL/PEA₂(MA)ₙ₋₁PbₙBr₃ₙ₊₁/ TPBI/LiF/Al	CE ≈ 4.9 cd A⁻¹, L ≈ 2935 cd m⁻²
	2016/06[22]		$PEA_2(MA)_{n-1}Pb_nI_{3n+1}$	ITO/TiO₂/PEA₂(MA)ₙ₋₁PbₙI₃ₙ₊₁/F8/ MoO₃/Au	EQE ≈ 8.8%, R ≈ 80 W sr⁻¹ m⁻²
	2016/09[87]		$NMA_2(FAPbI_3)_{n-1}PbI_4$	ITO/ZnO/PEIEᵃ⁾/NMA₂(FAPbI₃)ₙ₋₁PbI₄/ TFBᵇ⁾/MoOₓ/Au	EQE ≈ 11.7%, R ≈ 82 W sr⁻¹ m⁻²
	2017/01[47]		$BA_{0.17}MA_{0.83}PbBr_3$ $BA_{0.2857}MA_{0.7143}PbI_3$	ITO/PVK/BA₀.₁₇MA₀.₈₃PbBr₃/TPBI/LiF/Al ITO/poly-TPDᶜ⁾/BA₀.₂₈₅₇MA₀.₇₁₄₃PbI₃/TPBI/ LiF/Al	EQE ≈ 9.3%, 17.1 A⁻¹ EQE ≈ 10.4%
	2016/07[93]		$Cs_{0.87}MA_{0.13}PbBr_3$	ITO/ZnO/PVP/Cs₀.₈₇MA₀.₁₃PbBr₃/CBP/ MoO₃/Al	EQE ≈ 10.43%, CE ≈ 33.9 cd A⁻¹, L ≈ 91 000 cd m⁻²
	2016/11[97]	Two-step solution process	$FAPbBr_3$	ITO/ZnO/FAPbBr₃/poly-TPD/MoO₃/Al	EQE ≈ 1.16%, CE ≈ 2.65 cd A⁻¹, L ≈ 13 062 cd m⁻²
	2015/12[4]	Nanocrystal pinning process	$MAPbBr_3$	Polymeric anode/MAPbBr₃/TPBI/LiF/Al	EQE ≈ 8.52%, CE ≈ 42.9 cd A⁻¹
	2015/12[111]	Blade coating	$MAPbBr_3$:PEO	ITO/MAPbBr₃:PEO/Ag nanowires	EQE ≈ 1.1%, CE ≈ 4.91 cd A⁻¹, L ≈ 21 014 cd m⁻²
Vacuum-deposited PC bulk films	2015/09[36]	Coevaporation deposition	$MAPb(I_{0.6}Br_{0.4})_3$	ITO/PEDOT:PSS/ MAPb(I₀.₆Br₀.₄)₃/PCBMᵈ⁾/ Ba/Ag	EQE ≈ 0.06%
	2017/10[126]	Sequential vapor deposition	$(PEA)_2(MAPbBr_3)_nPbBr_4$	ITO/PEDOT:PSS/(PEA)₂(MAPbBr₃)ₙPbBr₄/ TPBI/LiF/Al	EQE ≈ 0.36%, CE ≈ 1.3 cd A⁻¹
	2017/06[132]	Chemical vapor deposition	$MAPbBr_3$	ITO/PFN-OXᵉ⁾/MAPbBr₃/TAPCᶠ⁾/MoO₃/Au	EQE ≈ 0.02%, CE ≈ 0.06 cd A⁻¹, L ≈ 900 cd m⁻²
	2017/11[41]	Vapor-assisted solution process	$MAPbBr_3$	ITO/P-NiO/MAPbBr₃/TPBI/LiF/Al	EQE ≈ 4.36%, CE ≈ 8.16 cd/A, L ≈ 6530 cd m⁻²
Colloidal NCs	2015/10[156]	Hot-injection method	$CsPbX_3$	ITO/PEDOT:PSS/PVK/ CsPbX₃/TPBI/LiF/Al	Blue: EQE ≈ 0.07%, CE ≈ 0.14 cd A⁻¹, L ≈ 742 cd m⁻² Green: EQE ≈ 0.12%, CE ≈ 0.43 cd A⁻¹, L ≈ 946 cd m⁻² Orange: EQE ≈ 0.09%, CE ≈ 0.08 cd A⁻¹, L ≈ 528 cd m⁻²

**ADVANCED
SCIENCE NEWS**
www.advancedsciencenews.com

**small
methods**
www.small-methods.com

Table 1. Continued.

Crystal forms	Publication date[ref]	Crystallization method	Emission layer	Device structure	EL efficiencies
	2016/11[158]		CsPbBr$_3$	ITO/PEDOT:PSS/poly-TPD/CsPbBr$_3$/TPBI/ LiF/Al	EQE ≈ 6.27%, CE ≈ 13.3 cd A^{-1}, L ≈ 15 185 cd m^{-2}
	2017/05[48]		CsPbBr$_3$	ITO/modified PEDOT:PSS/poly-TPD/ CsPbBr$_3$/TPBI/LiF/Al	EQE of 8.73%, CE of 18.8 cd A^{-1}
	2017/06[13]	Recrystallization methods	MAPbBr$_3$	ITO/buffer HIL/MAPbBr$_3$/TPBI/LiF/Al	EQE ≈ 5.09%, CE ≈ 15.5 cd A^{-1}
	2017/08[14]		FAPbBr$_3$	ITO/buffer HIL/FAPbBr$_3$/TPBI/LiF/Al	CE ≈ 9.16 cd A^{-1}
	2017/03[105]	In situ formation	MAPbBr$_3$:PEABr MAPbI$_3$:FPMAI	ITO/PEDOT:PSS/poly-TPD/MAPbBr$_3$:PEABr /TPBI/LiF/Al ITO/PEDOT:PSS/PVK/MAPbI$_3$:FPMAI / TPBI/LiF/Al	MAPbBr$_3$: EQE ≈ 7% MAPbI$_3$: EQE ≈ 7.9%
	2017/03[62]		MAPbBr$_3$:MABr	ITO/PEDOT:PSS/MAPbBr$_3$:MABr/TPBI/ LiF/Al	EQE ≈ 8.21%, CE ≈ 34.46 cd A^{-1}
SCs	2017/05[176]	Antisolvent vapor crystallization	MAPbBr$_3$	ITO/MAPbBr$_3$/Au	CE > 0.5 cd A^{-1}, L > 5000 cd m^{-2} at low temperature
	2017/09[49]	Chemical vapor deposition	MAPbBr$_3$	ITO/MAPbBr$_3$/ITO (lateral)	EQE ≈ 0.1–0.2%

a)PEIE: polyethylenimine ethoxylated; b)TFB: poly(9,9-dioctylfluorene-co-N-(4-butylphenyl) diphenylamine; c)poly-TPD: poly[bis(4-butypheny)-bis(phenyl)benzidine; d)PCBM: phenyl-C61-butyric acid methyl ester; e)PFN-OX: (6,6′-(9′,9′-Bis(6-((3-ethyloxetan-3-yl)methoxy)hexyl)-7,7′-diphenyl-9H,9′H-2,2′-bifluorene-9,9-diyl)bis(N,Ndiethylhexan-1-amine)); f)TAPC: (4,4′-Cyclohexylidenebis[N,N-bis(4-methylphenyl]benzenamine).

antisolvent (e.g., dichloromethane) into a perovskite precursor solution, SCs can be formed because the antisolvent steadily reduces the solubility of the perovskite precursors, and thereby induces crystallizaton (Figure 11c). MAPbBr$_3$ and MAPbI$_3$ SCs synthesized by AVC were found to show remarkably low trap densities of 5.8×10^9 and 3.3×10^{10} cm^{-3}, respectively.[180] Micrometer-sized MHP SCs synthesized by AVC methods can be applied on simplified PeLEDs (ITO/MHP SCs/Au) by forming cathodes and anodes directly on MHP SC microplatelets with lateral length of 20–100 µm and a thickness of 10 µm.[176] Ion migration induces intrinsic p–i–n junctions in MHP SC microplatelets at room temperature, and facilitates electron and hole injection from each electrode to the microplatelets. The p–i–n junction can be stabilized at low temperature; this makes PeLEDs based on micrometer-sized MHP SCs achieve CE > 0.5 cd A^{-1}, L > 5000 cd m^{-2}, and low V_{ON} ≈ 1.8 V.[176]

5.4. Inverse Temperature Crystallization

Inverse-temperature crystallization (ITC) exploits the solubility reduction of perovskite precursors in polar solvents (DMF, DMSO, GBL) with increasing solution temperature (Figure 11d). This method can synthesize MHP SCs much faster than can TSSG, BSSG, and AVC.[181] For this method, a large quantity of the perovskite precursor, such as MABr and PbBr$_2$, is dissolved in DMF at room temperature. Heating the perovskite solutions to 80 °C reduces the solubility of MAPbBr$_3$ in DMF from 0.8 to 0.3 g mL^{-1}; this solubility reduction induces supersaturation of perovskite precursors and crystallization into perovskite crystals. The growth rate of MHP SCs (MAPbI$_3$ and MAPbBr$_3$ SCs) increased gradually with increasing reaction time (≈3 mm^3 h^{-1} for the first hour), but ≈20 mm^3 h^{-1} (MAPbI$_3$ SCs) and ≈38 mm^3 h^{-1}

(MAPbBr$_3$ SCs), respectively, for the following hour).[181] The shapes of the MHP SCs can be controlled by choosing the geometry of the vessel in which crystallization occurs. SCs based on other MHPs, such as MAPbX$_3$,[182,183] FAPbX$_3$,[27,184,185] and FA$_{1-x}$MA$_x$PbX$_3$,[186–188] can be synthesized using ITC.

5.5. Chemical Vapor Deposition

MHP SCs can be also synthesized by CVD methods (Section 3.4).[49] These MHP SCs can be easily applied to PeLED applications because SCs can be formed directly on the patterned electrodes (Figure 11e). Rectangular micrometer-sized CsPbBr$_3$ SCs with lateral dimension ≈10 µm and thickness ≈100–500 nm were directly grown by CVD methods and placed between patterned ITO electrodes.[49] Under an applied bias, lateral structural PeLEDs with micrometer-sized CsPbBr$_3$ SCs showed pure green emission with an EL spectrum of 530–532 nm, FWHM of ≈22 nm, and EQE of 0.1–0.2%.[49]

6. Conclusion and Outlook

We have reviewed the recent progress in MHPs and PeLEDs by categorizing the forms of MHP emitters: i) PC bulk films, ii) colloidal NCs, and iii) SCs (**Table 1**). We have mainly focused on the various methods for the fabrication, synthesis, and modification of perovskite crystals, their photophysical properties, and application in PeLEDs. The low PLQE of MHP emitters and low EL efficiency of PeLEDs are mainly attributed to the fast dissociation of electron-hole pairs due to the small E_B, large grain size, and rough crystal morphologies; these problems can be solved by improving the MHP film morphology and by modifying the

perovskite crystals. Numerous and diverse research efforts have been tried, and thus greatly improved PLQE (>90% in NCs)[143] and EL efficiencies (EQE ≈ 14.36% in PC films,[46] EQE ≈ 8.73% in NCs,[48] and EQE ≈ 0.1–0.2% in SCs[49]) in each crystal form of MHP emitters have been achieved. However, these EL efficiencies of PeLEDs are still lower than those of OLEDs (EQE ≈ 30%),[8,31,32] QD LEDs (EQE ≈ 20%),[29,30] and the theoretically maximum device efficiency (EQE ≈ 25–30%), which can be calculated by considering the charge-balance factor (≈100%) and outcoupling efficiency (≈25–30%) in PeLEDs. Furthermore, there are still other challenges that must be overcome to achieve successful use of MHPs and PeLEDs.[189]

In MHP PC films, the LE can be increased by decreasing the grain size, but further reduction of the grain size to nanometer scales is currently very difficult. Furthermore, MHP PC films with a small grain size inevitably contain numerous grain boundaries, which can induce nonradiative recombination and reduce the LE of MHPs when no defect healing in grain boundaries is done. In MHP NCs, electron-hole pairs can be easily dissociated in film states due to the close proximity of the NCs; this process decreases the LE. Inspired by the progress of OLEDs, we suggest that dopant-in-host (MHP PC or NC-in-organic) systems[78] have potential to improve the EL efficiency of PeLEDs because these systems may further reduce the grain size, passivate surface defects in grain boundaries, and prevent dissociation of electron-hole pairs. Inspired by the progress of QD LEDs, core–shell[190] or gradient–alloy[191] (MHP NC–inorganic) system may also further confine the electron-hole pairs in their core perovskites and improve the EL efficiency.

The high sensitivity of MHP emitters to environmental conditions and low operating stability of PeLEDs must be solved from them to be used in industry.[189] Hydrophobic and crosslinkable organic cations or organic ligands can block the penetration of oxygen and moisture into perovskite crystals. Core–shell type (MHP NC–inorganic) NCs[190] can also show improved stability because the inorganic shell materials can have low oxygen permeability and prevent ion migration in the film states.

In addition, most MHPs use Pb atoms, which are toxic. Many researchers have tried to synthesize Pb-free or Pb-less MHP emitters and fabricate PeLEDs based on them. However, their LEs were much lower than Pb-based MHPs and PeLEDs due to the instability of the Pb-free MHPs. Adding Pb-free-MHP-crystal stabilizing agents during or after fabrication of the perovskite crystals can improve the stability and LE of Pb-free MHPs and PeLEDs based on them.

In summary, we believe that the ultimate goal of MHPs and PeLEDs is commercialization, and it will be achieved soon after solving the remaining problems, such as insufficient LE, sensitivity to environmental conditions, and low stability. We hope that this review will help researchers to understand the progress in development of MHP emitters, and inspire them to further concentrate on the development of PeLEDs.

Acknowledgements

Conflict of Interest

The authors declare no conflict of interest.

Keywords

[1] Y.-H. Kim, H. Cho, T.-W. Lee, *Proc. Natl. Acad. Sci. U. S. A.* **2016**, *113*, 11694.

[2] Y.-H. Kim, H. Cho, J. H. Heo, T.-S. Kim, N. Myoung, C.-L. Lee, S. H. Im, T.-W. Lee, *Adv. Mater.* **2015**, *27*, 1248.

[3] Z.-K. Tan, R. S. Moghaddam, M. L. Lai, P. Docampo, R. Higler, F. Deschler, M. Price, A. Sadhanala, L. M. Pazos, D. Credgington, F. Hanusch, T. Bein, H. J. Snaith, R. H. Friend, *Nat. Nanotechnol.* **2014**, *9*, 687.

[4] H. Cho, S.-H. Jeong, M.-H. Park, Y.-H. Kim, C. Wolf, C.-L. Lee, J. H. Heo, A. Sadhanala, N. Myoung, S. Yoo, S. H. Im, R. H. Friend, T.-W. Lee, *Science* **2015**, *350*, 1222.

[5] G. Xing, N. Mathews, S. S. Lim, N. Yantara, X. Liu, D. Sabba, M. Grätzel, S. Mhaisalkar, T. C. Sum, *Nat. Mater.* **2014**, *13*, 476.

[6] C. W. Tang, S. A. Vanslyke, C. H. Chen, *J. Appl. Phys.* **1989**, *65*, 3610.

[7] C. Adachi, M. A. Baldo, M. E. Thompson, S. R. Forrest, *J. Appl. Phys.* **2001**, *90*, 5048.

[8] Y.-H. Kim, C. Wolf, H. Cho, S.-H. Jeong, T.-W. Lee, *Adv. Mater.* **2016**, *28*, 734.

[9] V. L. Colvin, M. C. Schlamp, A. P. Alivisatos, *Nature* **1994**, *370*, 354.

[10] B. O. Dabbousi, M. G. Bawendi, O. Onitsuka, M. F. Rubner, *Appl. Phys. Lett.* **1995**, *66*, 1316.

[11] S. Coe, W.-K. Woo, M. Bawendi, V. Bulović, *Nature* **2002**, *420*, 800.

[12] H. Zhu, Y. Fu, F. Meng, X. Wu, Z. Gong, Q. Ding, M. V. Gustafsson, M. T. Trinh, S. Jin, X. Y. Zhu, *Nat. Mater.* **2015**, *14*, 636.

[13] Y.-H. Kim, C. Wolf, Y.-T. Kim, H. Cho, W. Kwon, S. Do, A. Sadhanala, C. G. Park, S.-W. Rhee, S. H. Im, R. H. Friend, T.-W. Lee, *ACS Nano* **2017**, *11*, 6586.

[14] Y.-H. Kim, G.-H. Lee, Y.-T. Kim, C. Wolf, H. J. Yun, W. Kwon, C. G. Park, T.-W. Lee, *Nano Energy* **2017**, *38*, 51.

[15] T. Hattori, T. Taira, M. Era, T. Tsutsui, S. Saito, *Chem. Phys. Lett.* **1996**, *254*, 103.

[16] I. Koutselas, P. Bampoulis, E. Maratou, T. Evagelinou, G. Pagona, G. C. Papavassiliou, *J. Phys. Chem. C* **2011**, *115*, 8475.

[17] K. Chondroudis, D. B. Mitzi, *Chem. Mater.* **1999**, *11*, 3028.

[18] I. B. Koutselas, L. Ducasse, G. C. Papavassiliou, *J. Phys.: Condens. Matter* **1996**, *8*, 1217.

[19] Z. Liu, Y. Bekenstein, X. Ye, S. C. Nguyen, J. Swabeck, D. Zhang, S.-T. Lee, P. Yang, W. Ma, A. P. Alivisatos, *J. Am. Chem. Soc.* **2017**, *139*, 5309.

[20] Y. Zhang, M. I. Saidaminov, I. Dursun, H. Yang, B. Murali, E. Alarousu, E. Yengel, B. A. Alshankiti, O. M. Bakr, O. F. Mohammed, *J. Phys. Chem. Lett.* **2017**, *8*, 961.

[21] J. Byun, H. Cho, C. Wolf, M. Jang, A. Sadhanala, R. H. Friend, H. Yang, T.-W. Lee, *Adv. Mater.* **2016**, *28*, 7515.

[22] M. Yuan, L. N. Quan, R. Comin, G. Walters, R. Sabatini, O. Voznyy, S. Hoogland, Y. Zhao, E. M. Beauregard, P. Kanjanaboos, Z. Lu, D. H. Kim, E. H. Sargent, *Nat. Nanotechnol.* **2016**, *11*, 872.

[23] S. Sun, D. Yuan, Y. Xu, A. Wang, Z. Deng, *ACS Nano* **2016**, *10*, 3648.

[24] T. Jeon, S. J. Kim, J. Yoon, J. Byun, H. R. Hong, T.-W. Lee, J.-S. Kim, B. Shin, S. O. Kim, *Adv. Energy Mater.* **2017**, *7*, 1602596.

[25] C. C. Stoumpos, C. D. Malliakas, J. A. Peters, Z. Liu, M. Sebastian, J. Im, T. C. Chasapis, A. C. Wibowo, D. Y. Chung, A. J. Freeman, B. W. Wessels, M. G. Kanatzidis, *Cryst. Growth Des.* **2013**, *13*, 2722.

[26] P. Schulz, E. Edri, S. Kirmayer, G. Hodes, D. Cahen, A. Kahn, *Energy Environ. Sci.* **2014**, *7*, 1377.

[27] A. A. Zhumekenov, M. I. Saidaminov, M. A. Haque, E. Alarousu, S. P. Sarmah, B. Murali, I. Dursun, X.-H. Miao, A. L. Abdelhady, T. Wu, O. F. Mohammed, O. M. Bakr, *ACS Energy Lett.* **2016**, *1*, 32.

[28] J. H. Heo, D. H. Song, S. H. Im, *Adv. Mater.* **2014**, *26*, 8179.

[29] X. Dai, Z. Zhang, Y. Jin, Y. Niu, H. Cao, X. Liang, L. Chen, J. Wang, X. Peng, *Nature* **2014**, *515*, 96.

[30] B. S. Mashford, M. Stevenson, Z. Popovic, C. Hamilton, Z. Zhou, C. Breen, J. Steckel, V. Bulovic, M. Bawendi, S. Coe-Sullivan, P. T. Kazlas, *Nat. Photonics* **2013**, *7*, 407.

[31] T.-H. Han, M.-R. Choi, S.-H. Woo, S.-Y. Min, C.-L. Lee, T.-W. Lee, *Adv. Mater.* **2012**, *24*, 1487.

[32] H. Uoyama, K. Goushi, K. Shizu, H. Nomura, C. Adachi, *Nature* **2012**, *492*, 234.

[33] G. Xing, B. Wu, X. Wu, M. Li, B. Du, Q. Wei, J. Guo, E. K. L. Yeow, T. C. Sum, W. Huang, *Nat. Commun.* **2017**, *8*, 14558.

[34] B. A. Koscher, J. K. Swabeck, N. D. Bronstein, A. P. Alivisatos, *J. Am. Chem. Soc.* **2017**, *139*, 6566.

[35] M. Liu, M. B. Johnston, H. J. Snaith, *Nature* **2013**, *501*, 395.

[36] L. Gil-Escrig, A. Miquel-Sempere, M. Sessolo, H. J. Bolink, *J. Phys. Chem. Lett.* **2015**, *6*, 3743.

[37] O. Malinkiewicz, C. Roldán-Carmona, A. Soriano, E. Bandiello, L. Camacho, M. K. Nazeeruddin, H. J. Bolink, *Adv. Energy Mater.* **2014**, *4*, 1400345.

[38] C. Momblona, L. Gil-Escrig, E. Bandiello, E. M. Hutter, M. Sessolo, K. Lederer, J. Blochwitz-Nimoth, H. J. Bolink, *Energy Environ. Sci.* **2016**, *9*, 3456.

[39] T. Matsushima, K. Fujita, T. Tsutsui, *Jpn. J. Appl. Phys.* **2005**, *44*, 1457.

[40] F. Hao, C. C. Stoumpos, Z. Liu, R. P. H. Chang, M. G. Kanatzidis, *J. Am. Chem. Soc.* **2014**, *136*, 16411.

[41] H. Ji, Z. Shi, X. Sun, Y. Li, S. Li, L. Lei, D. Wu, T. Xu, X. Li, G. Du, *ACS Appl. Mater. Interfaces* **2017**, *9*, 42893.

[42] Q. Chen, H. Zhou, Z. Hong, S. Luo, H.-S. Duan, H.-H. Wang, Y. Liu, G. Li, Y. Yang, *J. Am. Chem. Soc.* **2014**, *136*, 622.

[43] Z. Long, H. Ren, J. Sun, J. Ouyang, N. Na, *Chem. Commun.* **2017**, *53*, 9914.

[44] H. Huang, Q. Xue, B. Chen, Y. Xiong, J. Schneider, C. Zhi, H. Zhong, A. L. Rogach, *Angew. Chem., Int. Ed.* **2017**, *129*, 9699.

[45] Z.-Y. Zhu, Q.-Q. Yang, L.-F. Gao, L. Zhang, A.-Y. Shi, C.-L. Sun, Q. Wang, H.-L. Zhang, *J. Phys. Chem. Lett.* **2017**, *8*, 1610.

[46] X. Yang, X. Zhang, J. Deng, Z. Chu, Q. Jiang, J. Meng, P. Wang, L. Zhang, Z. Yin, J. You, *Nat. Commun.* **2018**, *9*, 570.

[47] Z. Xiao, R. A. Kerner, L. Zhao, N. L. Tran, K. M. Lee, T.-W. Koh, G. D. Scholes, B. P. Rand, *Nat. Photonics* **2017**, *11*, 108.

[48] T. Chiba, K. Hoshi, Y.-J. Pu, Y. Takeda, Y. Hayashi, S. Ohisa, S. Kawata, J. Kido, *ACS Appl. Mater. Interfaces* **2017**, *9*, 18054.

[49] X. Hu, H. Zhou, Z. Jiang, X. Wang, S. Yuan, J. Lan, Y. Fu, X. Zhang, W. Zheng, X. Wang, X. Zhu, L. Liao, G. Xu, S. Jin, A. Pan, *ACS Nano* **2017**, *11*, 9869.

[50] J. Yan, B. Zhang, Y. Chen, A. Zhang, X. Ke, *ACS Appl. Mater. Interfaces* **2016**, *8*, 12756.

[51] J. C. Yu, D. Bin Kim, E. D. Jung, B. R. Lee, M. H. Song, *Nanoscale* **2016**, *8*, 7036.

[52] J. Li, S. G. R. Bade, X. Shan, Z. Yu, *Adv. Mater.* **2015**, *27*, 5196.

[53] S. P. Senanayak, B. Yang, T. H. Thomas, N. Giesbrecht, W. Huang, E. Gann, B. Nair, K. Goedel, S. Guha, X. Moya, C. R. McNeill, P. Docampo, A. Sadhanala, R. H. Friend, H. Sirringhaus, *Sci. Adv.* **2017**, *3*, e1601935.

[54] G. Giorgi, J.-I. Fujisawa, H. Segawa, K. Yamashita, *J. Phys. Chem. C* **2015**, *119*, 4694.

[55] X. Wu, H. Yu, N. Li, F. Wang, H. Xu, N. Zhao, *J. Phys. Chem. C* **2015**, *119*, 1253.

[56] D. H. Fabini, T. Hogan, H. A. Evans, C. C. Stoumpos, M. G. Kanatzidis, R. Seshadri, *J. Phys. Chem. Lett.* **2016**, *7*, 376.

[57] M. Long, T. Zhang, Y. Chai, C. F. Ng, T. C. W. Mak, J. Xu, K. Yan, *Nat. Commun.* **2016**, *7*, 13503.

[58] K. Yan, M. Long, T. Zhang, Z. Wei, H. Chen, S. Yang, J. Xu, *J. Am. Chem. Soc.* **2015**, *137*, 4460.

[59] R. A. Kerner, L. Zhao, Z. Xiao, B. P. Rand, *J. Mater. Chem. A* **2016**, *4*, 8308.

[60] N. Ahn, D.-Y. Son, I.-H. Jang, S. M. Kang, M. Choi, N.-G. Park, *J. Am. Chem. Soc.* **2015**, *137*, 8696.

[61] X. Zhao, B. Zhang, R. Zhao, B. Yao, X. Liu, J. Liu, Z. Xie, *J. Phys. Chem. Lett.* **2016**, *7*, 4259.

[62] J.-W. Lee, Y. J. Choi, J.-M. Yang, S. Ham, S. K. Jeon, J. Y. Lee, Y.-H. Song, E. K. Ji, D.-H. Yoon, S. Seo, H. Shin, G. S. Han, H. S. Jung, D. Kim, N.-G. Park, *ACS Nano* **2017**, *11*, 3311.

[63] N. K. Kumawat, A. Dey, K. L. Narasimhan, D. Kabra, *ACS Photonics* **2015**, *2*, 349.

[64] E. Edri, S. Kirmayer, M. Kulbak, G. Hodes, D. Cahen, *J. Phys. Chem. Lett.* **2014**, *5*, 429.

[65] Z. Wei, A. Perumal, R. Su, S. Sushant, J. Xing, Q. Zhang, S. T. Tan, H. V. Demir, Q. Xiong, *Nanoscale* **2016**, *8*, 18021.

[66] Y.-J. Jeon, S. Lee, R. Kang, J.-E. Kim, J.-S. Yeo, S.-H. Lee, S.-S. Kim, J.-M. Yun, D.-Y. Kim, *Sci. Rep.* **2015**, *4*, 6953.

[67] P.-W. Liang, C.-Y. Liao, C.-C. Chueh, F. Zuo, S. T. Williams, X.-K. Xin, J. Lin, A. K.-Y. Jen, *Adv. Mater.* **2014**, *26*, 3748.

[68] Y. Chen, Y. Zhao, Z. Liang, *Chem. Mater.* **2015**, *27*, 1448.

[69] G. E. Eperon, S. D. Stranks, C. Menelaou, M. B. Johnston, L. M. Herz, H. J. Snaith, *Energy Environ. Sci.* **2014**, *7*, 982.

[70] N. Ahn, S. M. Kang, J.-W. Lee, M. Choi, N.-G. Park, *J. Mater. Chem. A* **2015**, *3*, 19901.

[71] A. E. Lewis, Y. Zhang, P. Gao, M. K. Nazeeruddin, *ACS Appl. Mater. Interfaces* **2017**, *9*, 25063.

[72] M. K. Kim, T. Jeon, H. I. Park, J. M. Lee, S. A. Nam, S. O. Kim, *CrystEngComm* **2016**, *18*, 6090.

[73] Y. Ling, Y. Tian, X. Wang, J. C. Wang, J. M. Knox, F. Perez-Orive, Y. Du, L. Tan, K. Hanson, B. Ma, H. Gao, *Adv. Mater.* **2016**, *28*, 8983.

[74] C. Wu, Y. Zou, T. Wu, M. Ban, V. Pecunia, Y. Han, Q. Liu, T. Song, S. Duhm, B. Sun, *Adv. Funct. Mater.* **2017**, *27*, 1700338.

[75] F. Meng, C. Zhang, D. Chen, W. Zhu, H.-L. Yip, S.-J. Su, *J. Mater. Chem. C* **2017**, *5*, 6169.

[76] G. Li, Z.-K. Tan, D. Di, M. L. Lai, L. Jiang, J. H.-W. Lim, R. H. Friend, N. C. Greenham, *Nano Lett.* **2015**, *15*, 2640.

[77] J. Li, X. Shan, S. G. R. Bade, T. Geske, Q. Jiang, X. Yang, Z. Yu, *J. Phys. Chem. Lett.* **2016**, *7*, 4059.

[78] P. Chen, Z. Xiong, X. Wu, M. Shao, X. Ma, Z.-H. Xiong, C. Gao, *J. Phys. Chem. Lett.* **2017**, *8*, 1810.

[79] P. D'Angelo, M. Barra, A. Cassinese, M. G. Maglione, P. Vacca, C. Minarini, A. Rubino, *Solid-State Electron.* **2007**, *51*, 123.

[80] G. Lin, H. Peng, L. Chen, H. Nie, W. Luo, Y. Li, S. Chen, R. Hu, A. Qin, Z. Zhao, B. Z. Tang, *ACS Appl. Mater. Interfaces* **2016**, *8*, 16799.

[81] Y. Zhao, J. Wei, H. Li, Y. Yan, W. Zhou, D. Yu, Q. Zhao, *Nat. Commun.* **2016**, *7*, 10228.

[82] D. Di, K. P. Musselman, G. Li, A. Sadhanala, Y. Ievskaya, Q. Song, Z.-K. Tan, M. L. Lai, J. L. MacManus-Driscoll, N. C. Greenham, R. H. Friend, *J. Phys. Chem. Lett.* **2015**, *6*, 446.

[83] J. Li, F. Cai, L. Yang, F. Ye, J. Zhang, R. S. Gurney, D. Liu, T. Wang, *Appl. Phys. Lett.* **2017**, *111*, 53301.

[84] K. Qasim, B. Wang, Y. Zhang, P. Li, Y. Wang, S. Li, S.-T. Lee, L.-S. Liao, W. Lei, Q. Bao, *Adv. Funct. Mater.* **2017**, *27*, 1606874.

[85] A. Baltakesmez, M. Biber, S. Tüzemen, *J. Appl. Phys.* **2017**, *122*, 85502.

ADVANCED
SCIENCE NEWS

www.advancedsciencenews.com

small
methods

www.small-methods.com

[86] Z. Chen, C. Zhang, X.-F. Jiang, M. Liu, R. Xia, T. Shi, D. Chen, Q. Xue, Y.-J. Zhao, S. Su, H.-L. Yip, Y. Cao, *Adv. Mater.* **2017**, *29*, 1603157.

[87] N. Wang, L. Cheng, R. Ge, S. Zhang, Y. Miao, W. Zou, C. Yi, Y. Sun, Y. Cao, R. Yang, Y. Wei, Q. Guo, Y. Ke, M. Yu, Y. Jin, Y. Liu, Q. Ding, D. Di, L. Yang, G. Xing, H. Tian, C. Jin, F. Gao, R. H. Friend, J. Wang, W. Huang, *Nat. Photonics* **2016**, *10*, 699.

[88] D. Liang, Y. Peng, Y. Fu, M. J. Shearer, J. Zhang, J. Zhai, Y. Zhang, R. J. Hamers, T. L. Andrew, S. Jin, *ACS Nano* **2016**, *10*, 6897.

[89] D. N. Congreve, M. C. Weidman, M. Seitz, W. Paritmongkol, N. S. Dahod, W. A. Tisdale, *ACS Photonics* **2017**, *4*, 476.

[90] C. Yi, J. Luo, S. Meloni, A. Boziki, N. Ashari-Astani, C. Grätzel, S. M. Zakeeruddin, U. Röthlisberger, M. Grätzel, *Energy Environ. Sci.* **2016**, *9*, 656.

[91] Z. Li, M. Yang, J.-S. Park, S.-H. Wei, J. J. Berry, K. Zhu, *Chem. Mater.* **2016**, *28*, 284.

[92] J.-W. Lee, D.-H. Kim, H.-S. Kim, S.-W. Seo, S. M. Cho, N.-G. Park, *Adv. Energy Mater.* **2015**, *5*, 1501310.

[93] L. Zhang, X. Yang, Q. Jiang, P. Wang, Z. Yin, X. Zhang, H. Tan, Y. M. Yang, M. Wei, B. R. Sutherland, E. H. Sargent, J. You, *Nat. Commun.* **2017**, *8*, 15640.

[94] N. J. Jeon, J. H. Noh, W. S. Yang, Y. C. Kim, S. Ryu, J. Seo, S. I. Seok, *Nature* **2014**, *517*, 476.

[95] H. P. Kim, J. Kim, B. S. Kim, H.-M. Kim, J. Kim, A. R. bin, M. Yusoff, J. Jang, M. K. Nazeeruddin, *Adv. Opt. Mater.* **2017**, *5*, 1600920.

[96] J. Si, Y. Liu, N. Wang, M. Xu, J. Li, H. He, J. Wang, Y. Jin, *Nano Res.* **2017**, *10*, 1329.

[97] L. Meng, E.-P. Yao, Z. Hong, H. Chen, P. Sun, Z. Yang, G. Li, Y. Yang, *Adv. Mater.* **2017**, *29*, 1603826.

[98] N. K. Kumawat, N. Jain, A. Dey, K. L. Narasimhan, D. Kabra, *Adv. Funct. Mater.* **2017**, *27*, 1603219.

[99] Y. Cheng, H.-W. Li, J. Zhang, Q.-D. Yang, T. Liu, Z. Guan, J. Qing, C.-S. Lee, S.-W. Tsang, *J. Mater. Chem. A* **2016**, *4*, 561.

[100] Y. Wu, A. Islam, X. Yang, C. Qin, J. Liu, K. Zhang, W. Peng, L. Han, *Energy Environ. Sci.* **2014**, *7*, 2934.

[101] J. Wu, X. Xu, Y. Zhao, J. Shi, Y. Xu, Y. Luo, D. Li, H. Wu, Q. Meng, *ACS Appl. Mater. Interfaces* **2017**, *9*, 26937.

[102] J.-H. Im, I.-H. Jang, N. Pellet, M. Grätzel, N.-G. Park, *Nat. Nanotechnol.* **2014**, *9*, 927.

[103] Y.-K. Chih, J.-C. Wang, R.-T. Yang, C.-C. Liu, Y.-C. Chang, Y.-S. Fu, W.-C. Lai, P. Chen, T.-C. Wen, Y.-C. Huang, C.-S. Tsao, T.-F. Guo, *Adv. Mater.* **2016**, *28*, 8687.

[104] J. C. Yu, D. W. Kim, D. Bin Kim, E. D. Jung, K.-S. Lee, S. Lee, D. Di Nuzzo, J.-S. Kim, M. H. Song, *Nanoscale* **2017**, *9*, 2088.

[105] L. Zhao, Y.-W. Yeh, N. L. Tran, F. Wu, Z. Xiao, R. A. Kerner, Y. L. Lin, G. D. Scholes, N. Yao, B. P. Rand, *ACS Nano* **2017**, *11*, 3957.

[106] H. Back, J. Kim, G. Kim, T. Kyun Kim, H. Kang, J. Kong, S. Ho Lee, K. Lee, *Sol. Energy Mater. Sol. Cells* **2016**, *144*, 309.

[107] Y. Deng, Q. Dong, C. Bi, Y. Yuan, J. Huang, *Adv. Energy Mater.* **2016**, *6*, 1600372.

[108] Y. Deng, E. Peng, Y. Shao, Z. Xiao, Q. Dong, J. Huang, *Energy Environ. Sci.* **2015**, *8*, 1544.

[109] S. Tong, H. Wu, C. Zhang, S. Li, C. Wang, J. Shen, S. Xiao, J. He, J. Yang, J. Sun, Y. Gao, *Org. Electron.* **2017**, *49*, 347.

[110] S. Razza, F. Di Giacomo, F. Matteocci, L. Cinà, A. L. Palma, S. Casaluci, P. Cameron, A. D'Epifanio, S. Licoccia, A. Reale, T. M. Brown, A. Di Carlo, *J. Power Sources* **2015**, *277*, 286.

[111] S. G. R. Bade, J. Li, X. Shan, Y. Ling, Y. Tian, T. Dilbeck, T. Besara, T. Geske, H. Gao, B. Ma, K. Hanson, T. Siegrist, C. Xu, Z. Yu, *ACS Nano* **2016**, *10*, 1795.

[112] Q. Hu, H. Wu, J. Sun, D. Yan, Y. Gao, J. Yang, *Nanoscale* **2016**, *8*, 5350.

[113] K. Hwang, Y.-S. Jung, Y.-J. Heo, F. H. Scholes, S. E. Watkins, J. Subbiah, D. J. Jones, D.-Y. Kim, D. Vak, *Adv. Mater.* **2015**, *27*, 1241.

[114] Y.-S. Jung, K. Hwang, Y.-J. Heo, J.-E. Kim, D. Lee, C.-H. Lee, H.-I. Joh, J.-S. Yeo, D.-Y. Kim, *ACS Appl. Mater. Interfaces* **2017**, *9*, 27832.

[115] A. T. Barrows, A. J. Pearson, C. K. Kwak, A. D. F. Dunbar, A. R. Buckley, D. G. Lidzey, *Energy Environ. Sci.* **2014**, *7*, 2944.

[116] P. S. Chandrasekhar, N. Kumar, S. K. Swami, V. Dutta, V. K. Komarala, *Nanoscale* **2016**, *8*, 6792.

[117] S. Das, B. Yang, G. Gu, P. C. Joshi, I. N. Ivanov, C. M. Rouleau, T. Aytug, D. B. Geohegan, K. Xiao, *ACS Photonics* **2015**, *2*, 680.

[118] S. Gamliel, A. Dymshits, S. Aharon, E. Terkieltaub, L. Etgar, *J. Phys. Chem. C* **2015**, *119*, 19722.

[119] D. K. Mohamad, J. Griffin, C. Bracher, A. T. Barrows, D. G. Lidzey, *Adv. Energy Mater.* **2016**, *6*, 1600994.

[120] J. H. Kim, S. T. Williams, N. Cho, C.-C. Chueh, A. K.-Y. Jen, *Adv. Energy Mater.* **2015**, *5*, 1401229.

[121] D. B. Mitzi, *Chem. Mater.* **2001**, *13*, 3283.

[122] M. Era, T. Hattori, T. Taira, T. Tsutsui, *Chem. Mater.* **1997**, *9*, 8.

[123] C.-W. Chen, H.-W. Kang, S.-Y. Hsiao, P.-F. Yang, K.-M. Chiang, H.-W. Lin, *Adv. Mater.* **2014**, *26*, 6647.

[124] A. Ng, Z. Ren, Q. Shen, S. H. Cheung, H. C. Gokkaya, G. Bai, J. Wang, L. Yang, S. K. So, A. B. Djurišić, W. W. Leung, J. Hao, W. K. Chan, C. Surya, *J. Mater. Chem. A* **2015**, *3*, 9223.

[125] H. Hu, D. Wang, Y. Zhou, J. Zhang, S. Lv, S. Pang, X. Chen, Z. Liu, N. P. Padture, G. Cui, *RSC Adv.* **2014**, *4*, 28964.

[126] K.-M. Chiang, B.-W. Hsu, Y.-A. Chang, L. Yang, W.-L. Tsai, H.-W. Lin, *ACS Appl. Mater. Interfaces* **2017**, *9*, 40516.

[127] Y. Zhao, K. Zhu, *J. Am. Chem. Soc.* **2014**, *136*, 12241.

[128] Y.-H. Kim, H. Cho, J. H. Heo, S. H. Im, T.-W. Lee, *Curr. Appl. Phys.* **2016**, *16*, 1069.

[129] G. Longo, L. Gil-Escrig, M. J. Degen, M. Sessolo, H. J. Bolink, *Chem. Commun.* **2015**, *51*, 7376.

[130] D. B. Mitzi, M. T. Prikas, K. Chondroudis, *Chem. Mater.* **1999**, *11*, 542.

[131] M. R. Leyden, Y. Jiang, Y. Qi, *J. Mater. Chem. A* **2016**, *4*, 13125.

[132] M. R. Leyden, L. Meng, Y. Jiang, L. K. Ono, L. Qiu, E. J. Juarez-Perez, C. Qin, C. Adachi, Y. Qi, *J. Phys. Chem. Lett.* **2017**, *8*, 3193.

[133] M. R. Leyden, M. V. Lee, S. R. Raga, Y. Qi, *J. Mater. Chem. A* **2015**, *3*, 16097.

[134] P. Luo, Z. Liu, W. Xia, C. Yuan, J. Cheng, Y. Lu, *ACS Appl. Mater. Interfaces* **2015**, *7*, 2708.

[135] D. S. Bhachu, D. O. Scanlon, E. J. Saban, H. Bronstein, I. P. Parkin, C. J. Carmalt, R. G. Palgrave, *J. Mater. Chem. A* **2015**, *3*, 9071.

[136] O. Malinkiewicz, A. Yella, Y. H. Lee, G. M. Espallargas, M. Graetzel, M. K. Nazeeruddin, H. J. Bolink, *Nat. Photonics* **2014**, *8*, 128.

[137] Q. Lin, A. Armin, R. C. R. Nagiri, P. L. Burn, P. Meredith, *Nat. Photonics* **2015**, *9*, 106.

[138] M. Kulbak, S. Gupta, N. Kedem, I. Levine, T. Bendikov, G. Hodes, D. Cahen, *J. Phys. Chem. Lett.* **2016**, *7*, 167.

[139] M. R. Leyden, L. K. Ono, S. R. Raga, Y. Kato, S. Wang, Y. Qi, *J. Mater. Chem. A* **2014**, *2*, 18742.

[140] A. Kojima, M. Ikegami, K. Teshima, T. Miyasaka, *Chem. Lett.* **2012**, *41*, 397.

[141] D. N. Dirin, L. Protesescu, D. Trummer, I. V. Kochetygov, S. Yakunin, F. Krumeich, N. P. Stadie, M. V. Kovalenko, *Nano Lett.* **2016**, *16*, 5866.

[142] T. Kollek, D. Gruber, J. Gehring, E. Zimmermann, L. Schmidt-Mende, S. Polarz, *Angew. Chem., Int. Ed.* **2015**, *54*, 1341.

[143] L. Protesescu, S. Yakunin, M. I. Bodnarchuk, F. Krieg, R. Caputo, C. H. Hendon, R. X. Yang, A. Walsh, M. V. Kovalenko, *Nano Lett.* **2015**, *15*, 3692.

[144] J. Pan, Y. Shang, J. Yin, M. De Bastiani, W. Peng, I. Dursun, L. Sinatra, A. M. El-Zohry, M. N. Hedhili, A.-H. Emwas, O. F. Mohammed, Z. Ning, O. M. Bakr, *J. Am. Chem. Soc.* **2018**, *140*, 562.

[145] J. Shamsi, Z. Dang, P. Bianchini, C. Canale, F. Di Stasio, R. Brescia, M. Prato, L. Manna, *J. Am. Chem. Soc.* **2016**, *138*, 7240.

**ADVANCED
SCIENCE NEWS**

www.advancedsciencenews.com

**small
methods**

www.small-methods.com

[146] A. Pan, B. He, X. Fan, Z. Liu, J. J. Urban, A. P. Alivisatos, L. He, Y. Liu, *ACS Nano* **2016**, *10*, 7943.

[147] G. H. Ahmed, J. Yin, R. Bose, L. Sinatra, E. Alarousu, E. Yengel, N. M. Alyami, M. I. Saidaminov, Y. Zhang, M. N. Hedhili, O. M. Bakr, J.-L. Brédas, O. F. Mohammed, *Chem. Mater.* **2017**, *29*, 4393.

[148] D. Zhang, Y. Yu, Y. Bekenstein, A. B. Wong, A. P. Alivisatos, P. Yang, *J. Am. Chem. Soc.* **2016**, *138*, 13155.

[149] Y. Tong, B. J. Bohn, E. Bladt, K. Wang, P. Müller-Buschbaum, S. Bals, A. S. Urban, L. Polavarapu, J. Feldmann, *Angew. Chem., Int. Ed.* **2017**, *56*, 13887.

[150] J. A. Sichert, Y. Tong, N. Mutz, M. Vollmer, S. Fischer, K. Z. Milowska, R. García Cortadella, B. Nickel, C. Cardenas-Daw, J. K. Stolarczyk, A. S. Urban, J. Feldmann, *Nano Lett.* **2015**, *15*, 6521.

[151] Q. A. Akkerman, S. G. Motti, A. R. Srimath Kandada, E. Mosconi, V. D'Innocenzo, G. Bertoni, S. Marras, B. A. Kamino, L. Miranda, F. De Angelis, A. Petrozza, M. Prato, L. Manna, *J. Am. Chem. Soc.* **2016**, *138*, 1010.

[152] Z. Dang, J. Shamsi, F. Palazon, M. Imran, Q. A. Akkerman, S. Park, G. Bertoni, M. Prato, R. Brescia, L. Manna, *ACS Nano* **2017**, *11*, 2124.

[153] J. Shamsi, P. Rastogi, V. Caligiuri, A. L. Abdelhady, D. Spirito, L. Manna, R. Krahne, *ACS Nano* **2017**, *11*, 10206.

[154] Y. Wang, X. Li, S. Sreejith, F. Cao, Z. Wang, M. C. Stuparu, H. Zeng, H. Sun, *Adv. Mater.* **2016**, *28*, 10637.

[155] L. Wang, K. Wang, B. Zou, *J. Phys. Chem. Lett.* **2016**, *7*, 2556.

[156] J. Song, J. Li, X. Li, L. Xu, Y. Dong, H. Zeng, *Adv. Mater.* **2015**, *27*, 7162.

[157] J. Pan, L. N. Quan, Y. Zhao, W. Peng, B. Murali, S. P. Sarmah, M. Yuan, L. Sinatra, N. M. Alyami, J. Liu, E. Yassitepe, Z. Yang, O. Voznyy, R. Comin, M. N. Hedhili, O. F. Mohammed, Z. H. Lu, D. H. Kim, E. H. Sargent, O. M. Bakr, *Adv. Mater.* **2016**, *28*, 8718.

[158] J. Li, L. Xu, T. Wang, J. Song, J. Chen, J. Xue, Y. Dong, B. Cai, Q. Shan, B. Han, H. Zeng, *Adv. Mater.* **2017**, *29*, 1603885.

[159] X. Li, Y. Wu, S. Zhang, B. Cai, Y. Gu, J. Song, H. Zeng, *Adv. Funct. Mater.* **2016**, *26*, 2435.

[160] F. Zhang, H. Zhong, C. Chen, X. Wu, X. Hu, H. Huang, J. Han, B. Zou, Y. Dong, *ACS Nano* **2015**, *9*, 4533.

[161] A. Perumal, S. Shendre, M. Li, Y. K. E. Tay, V. K. Sharma, S. Chen, Z. Wei, Q. Liu, Y. Gao, P. J. S. Buenconsejo, S. T. Tan, C. L. Gan, Q. Xiong, T. C. Sum, H. V. Demir, *Sci. Rep.* **2016**, *6*, 36733.

[162] H. Huang, A. S. Susha, S. V Kershaw, T. F. Hung, A. L. Rogach, *Adv. Sci.* **2015**, *2*, 1500194.

[163] Y. Ling, Z. Yuan, Y. Tian, X. Wang, J. C. Wang, Y. Xin, K. Hanson, B. Ma, H. Gao, *Adv. Mater.* **2016**, *28*, 305.

[164] H. Sun, Z. Yang, M. Wei, W. Sun, X. Li, S. Ye, Y. Zhao, H. Tan, E. L. Kynaston, T. B. Schon, H. Yan, Z.-H. Lu, G. A. Ozin, E. H. Sargent, D. S. Seferos, *Adv. Mater.* **2017**, *29*, 1701153.

[165] S. Kumar, J. Jagielski, N. Kallikounis, Y.-H. Kim, C. Wolf, F. Jenny, T. Tian, C. J. Hofer, Y.-C. Chiu, W. J. Stark, T.-W. Lee, C.-J. Shih, *Nano Lett.* **2017**, *17*, 5277.

[166] W. Deng, X. Xu, X. Zhang, Y. Zhang, X. Jin, L. Wang, S.-T. Lee, J. Jie, *Adv. Funct. Mater.* **2016**, *26*, 4797.

[167] Q. Pan, H. Hu, Y. Zou, M. Chen, L. Wu, D. Yang, X. Yuan, J. Fan, B. Sun, Q. Zhang, *J. Mater. Chem. C* **2017**, *5*, 10947.

[168] Y. Tong, E. Bladt, M. F. Aygüler, A. Manzi, K. Z. Milowska, V. A. Hintermayr, P. Docampo, S. Bals, A. S. Urban, L. Polavarapu, J. Feldmann, *Angew. Chem., Int. Ed.* **2016**, *55*, 13887.

[169] V. A. Hintermayr, A. F. Richter, F. Ehrat, M. Döblinger, W. Vanderlinden, J. A. Sichert, Y. Tong, L. Polavarapu, J. Feldmann, A. S. Urban, *Adv. Mater.* **2016**, *28*, 9478.

[170] Q. Dong, Y. Fang, Y. Shao, P. Mulligan, J. Qiu, L. Cao, J. Huang, *Science* **2015**, *347*, 967.

[171] Y. Dang, Y. Zhou, X. Liu, D. Ju, S. Xia, H. Xia, X. Tao, *Angew. Chem., Int. Ed.* **2016**, *128*, 3508.

[172] Y. Bi, E. M. Hutter, Y. Fang, Q. Dong, J. Huang, T. J. Savenije, *J. Phys. Chem. Lett.* **2016**, *7*, 923.

[173] W. Peng, L. Wang, B. Murali, K.-T. Ho, A. Bera, N. Cho, C. F. Kang, V. M. Burlakov, J. Pan, L. Sinatra, C. Ma, W. Xu, D. Shi, E. Alarousu, A. Goriely, J.-H. He, O. F. Mohammed, T. Wu, O. M. Bakr, *Adv. Mater.* **2016**, *28*, 3383.

[174] Y.-X. Chen, Q.-Q. Ge, Y. Shi, J. Liu, D.-J. Xue, J.-Y. Ma, J. Ding, H.-J. Yan, J.-S. Hu, L.-J. Wan, *J. Am. Chem. Soc.* **2016**, *138*, 16196.

[175] J. Chen, D. J. Morrow, Y. Fu, W. Zheng, Y. Zhao, L. Dang, M. J. Stolt, D. D. Kohler, X. Wang, K. J. Czech, M. P. Hautzinger, S. Shen, L. Guo, A. Pan, J. C. Wright, S. Jin, *J. Am. Chem. Soc.* **2017**, *139*, 13525.

[176] M. Chen, X. Shan, T. Geske, J. Li, Z. Yu, *ACS Nano* **2017**, *11*, 6312.

[177] Y. Dang, Y. Liu, Y. Sun, D. Yuan, X. Liu, W. Lu, G. Liu, H. Xia, X. Tao, *CrystEngComm* **2015**, *17*, 665.

[178] Y. Dang, D. Ju, L. Wang, X. Tao, *CrystEngComm* **2016**, *18*, 4476.

[179] Y. Dang, C. Zhong, G. Zhang, D. Ju, L. Wang, S. Xia, H. Xia, X. Tao, *Chem. Mater.* **2016**, *28*, 6968.

[180] D. Shi, V. Adinolfi, R. Comin, M. Yuan, E. Alarousu, A. Buin, Y. Chen, S. Hoogland, A. Rothenberger, K. Katsiev, Y. Losovyj, X. Zhang, P. A. Dowben, O. F. Mohammed, E. H. Sargent, O. M. Bakr, *Science* **2015**, *347*, 519.

[181] M. I. Saidaminov, A. L. Abdelhady, B. Murali, E. Alarousu, V. M. Burlakov, W. Peng, I. Dursun, L. Wang, Y. He, G. Maculan, A. Goriely, T. Wu, O. F. Mohammed, O. M. Bakr, *Nat. Commun.* **2015**, *6*, 7586.

[182] G. Maculan, A. D. Sheikh, A. L. Abdelhady, M. I. Saidaminov, M. A. Haque, B. Murali, E. Alarousu, O. F. Mohammed, T. Wu, O. M. Bakr, *J. Phys. Chem. Lett.* **2015**, *6*, 3781.

[183] F. Zhang, B. Yang, X. Mao, R. Yang, L. Jiang, Y. Li, J. Xiong, Y. Yang, R. He, W. Deng, K. Han, *ACS Appl. Mater. Interfaces* **2017**, *9*, 14827.

[184] M. I. Saidaminov, A. L. Abdelhady, G. Maculan, O. M. Bakr, *Chem. Commun.* **2015**, *51*, 17658.

[185] Y. Liu, J. Sun, Z. Yang, D. Yang, X. Ren, H. Xu, Z. Yang, S. F. Liu, *Adv. Opt. Mater.* **2016**, *4*, 1829.

[186] Y. Huang, L. Li, Z. Liu, H. Jiao, Y. He, X. Wang, R. Zhu, D. Wang, J. Sun, Q. Chen, H. Zhou, *J. Mater. Chem. A* **2017**, *5*, 8537.

[187] L.-Q. Xie, L. Chen, Z.-A. Nan, H.-X. Lin, T. Wang, D.-P. Zhan, J.-W. Yan, B.-W. Mao, Z.-Q. Tian, *J. Am. Chem. Soc.* **2017**, *139*, 3320.

[188] O. Nazarenko, S. Yakunin, V. Morad, I. Cherniukh, M. V Kovalenko, *NPG Asia Mater.* **2017**, *9*, e373.

[189] H. Cho, Y.-H. Kim, C. Wolf, H.-D. Lee, T.-W. Lee, *Adv. Mater.* **2018**, https://doi.org/10.1002/adma.201704587.

[190] T.-W. Lee, S. H. Im, Y.-H. Kim, H. Cho (POSTECH ACADEMY-INDUSTRY FOUNDATION), *PCT/KR2015/011960*, **2015**.

[191] T.-W. Lee, S. H. Im, Y.-H. Kim, H. Cho (POSTECH ACADEMY-INDUSTRY FOUNDATION), *PCT/KR2015/011962*, **2015**.